Observation of the Peculiar Properties of $MgTiO_2$ coated TCO substrates

By

SUJITHA B

(20PPH023)

A Thesis submitted to

Avinashilingam Institute for Home Science and Higher Education for Women

Coimbatore – 641043

In Partial Fulfilment of the Requirements for the Degree of

MASTER OF SCIENCE IN PHYSICS

MAY 2022

Observation of the Peculiar Properties of $MgTiO_2$ coated TCO substrates

By

SUJITHA B

(20PPH023)

A Thesis submitted to

Avinashilingam Institute for Home Science and Higher Education for Women

Coimbatore – 641043

In Partial Fulfilment of the Requirements for the Degree of

MASTER OF SCIENCE IN PHYSICS

MAY 2022

CERTIFIED AS A BONAFIDE RESEARCH WORK

27/05/22

Signature of Head of the Department

27/5/22

Signature of the Supervisor

DECLARATION

I hereby declare that the project work entitled " Observation of the Peculiar Properties of $MgTiO_2$ coated TCO substrates " submitted to the Department of Physics, Avinashilingam Institute for Home Science and Higher Education for Women, Coimbatore, is a record of an original work done by me under the guidance of **Dr. Mrs. G.Kiruthiga**, M.Sc., M.Phil., PGDCA(Ph.D.), Assistant Professor, Department of Physics, and the project work is submitted in the fulfilment of the requirements for the degree of Master of Science in Physics. The results embodied in this have not been submitted to any other university or Institute for the award of any degree or diploma.

SUJITHA B

(20PPH023)

ACKNOWLEDGEMENT

We owe our sincere thanks to **Lord Almighty** and **my lovable parents**. Without whom we should have been nothing, for showering their generous blessings upon us in all endeavours.

We wish to express our deep sense of reverential gratitude to, **Prof. S.P. Thyagarajan**, Chancellor of Avinashilingam Institute for Home Science and Higher Education for Women, Coimbatore, for providing the facilities performing the major project.

We sincerely thank **Dr. (Mrs) V.Bharathi Harishankar**, Ph.D., FRSA., Vice Chancellor of Avinashilingam Institute for Home Science and Higher Education for Women, Coimbatore, for providing all the necessary facilities for performing major project.

We heartily thank **Dr. (Mrs) S.Kowsalya**, M.Sc., M.Phil., PhD., Registrar of Avinashilingam Institute for Home Science and Higher Education for Women, Coimbatore for providing adequate facilities required to carry out the major project.

We whole heartily thank **Dr. (Mrs) G.Padmavathi**, M.Sc., M.Phil., Ph.D., Dean, School of Physical Sciences and Computational Sciences, Avinashilingam Institute for Home Science and Higher Education for Women, Coimbatore for her encouragement and generous help which was of a great value.

We express our sincere gratitude to **Dr. (Mrs) J.Shanthi**, M.Sc., M.Phil., Ph.D., Professor and Head of the Department of Physics, Avinashilingam Institute for Home Science and Higher Education for Women, Coimbatore for her constant support and encouragement for all our activities.

I run ever grateful to my Guide **Dr. Mrs. G.Kiruthiga**, M.Sc., M.Phil., PGDCA(Ph.D.), Assistant Professor, Department of Physics, Avinashilingam Institute for Home Science and Higher Education for Women, Coimbatore, for her excellent, outstanding guidance, constructive criticism, motivation, valuable advice, untiring support ,timely suggestions, constant encouragement, and inspiration throughout the study, holding me strong in all the places I faltered.

We also thank all other staff members of Department of Physics, Avinashilingam Institute for Home Science and Higher Education for Women, Coimbatore for being supportive on all our activities.

SUJITHA B

CONTENTS

LIST OF FIGURES

LIST OF TABLES

CHAPTER I
INTRODUCTION

1.1. INTRODUCTION:

The existing of mankind depends on the need of energy[1]. Energy demand of the world have been decreasing constantly due to the urbanization and commercialization. Most demands of energy are fulfilled by the use of fossil fuel[2]. The available resources can be categorized into two, they are Non-renewable energy resources and Renewable energy resources. In non renewable resource, the energy can be generated by exploiting the sources which was regenerated in a long time. Coal, Fossil fuels, Natural gases fall under the category of non renewable energy resources. But the energy obtained from the non renewable sources are high. Renewable energy resources are instantly regenerated after use, that is the energy source does not exhaust. Tidal energy,geothermal energy,wind energy,solar energy and hydro-thermal energy falls under the category of the renewable energy sources. Among these renewable energy sources,solar energies has a lot of interest among the scientists[1]. Non renewable resource fossil fuel satisfy about 85% of world's energy requirement. The increase in the energy demand will be more by 2050 according to the He. Tang et al. in 2017[3]. About 35% of the total global energy is used for the residential and commercial purpose[4]. Due to the abundance, low cost, and environmental friendliness, solar energy grabs more attention from all over the world, which makes the rapid development of solar cell research[3]. The energy provided by the Sun in the form of light . The thought to convert sunlight into a form of energy is the basic concept of the solar cell[1]. Solar energy is renewable, environmentally clean, free and available in competent amount in almost all habitable parts of the world[5]. Energy from the Sun have been used in the form of electricity. Solar cell works on the principle of Photo-voltaic effect which converts sun light directly into electricity. In this work the thin film was developed using the nebulizer spray pyrolysis . In this work we have briefly studied about the sun, the photo electric current about the solar cells and their working principle. In this work Mg doped TiO_2 electrode (Photo anode) was coated on the TCO's using spray pyrolysis method. The preparation method and the methodology was discussed in the upcoming chapters.

1.2. SUN AND THE EARTH:

The Sun is the centre and the heart of the solar system. It is a star that is burning for about 4 billion years and is the nearest star around the Earth. Sun is responsible for almost all available energy on the Earth everything is converted from the Sun's energy. Hydropower is the evaporation-transpiration due to solar radiant heat. The winds are originated by the sun's uneven heating of the Earth's atmosphere; fossil fuels are residue of organic life previously nourished by the Sun. Photo-voltaic current is produced directly from sunlight by converting the energy in the sunlight into charged particles within certain kinds of materials.The sun's light is made up of many different colors that,

combined, produce a white light. Each visible and invisible radiations of the Sun's spectrum has a different energy. The atmosphere reduces many parts of the spectrum. X-rays are totally absorbed before reaching the ground. A good proportion of ultraviolet radiation is filtered out by the atmosphere. In the winter the sun will provide less than 20% of the summer sun's energy at some areas because it is lower in the sky and the days are even shorter. All these factors that affect the amount of local radiation on earth have taken into account on designing photo-voltaic systems. A good PV system cannot be designed without furnish for the variations associated with the energy spectrum and its local availability[6].

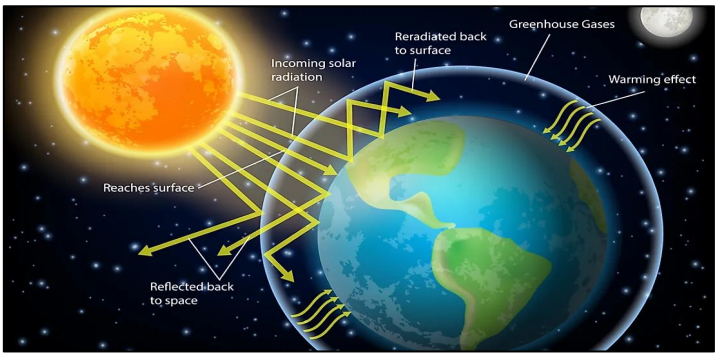

Figure 1.1. Solar radiation on the surface of the Earth

1.3. THE SOLAR CELL :

A device that converts the energy of light directly into electrical energy through the photovoltaic effect is the solar cell which is also known as photo voltaic cell.Solar cells are arranged into large groups called arrays[7].When light falls on a photo voltaic (PV) cell light may be reflected, absorbed through the cell. The PV cell is a semiconductor material; the word “semi” means that it can conduct electricity better than an insulator but not as good as a conductor like a metal. There are various semiconductor materials used in PV cells[8].

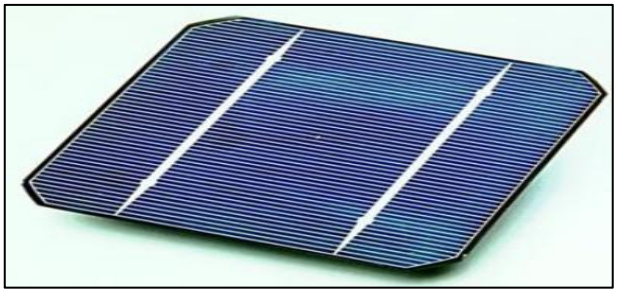

Fig 1.2. Solar Cell Fabrication

1.3.1. *PHOTO VOLTAIC EFFECT:*

When the semiconductor is exposed to light, it absorbs the sun’s light energy and transfers it to a negatively charged particles called electrons. The electrons flow through the material as an electrical current.The efficiency of a PV cell is the ratio of electrical power produced by the cell to the energy emitted by the light shining on it, indicating how efficient the cell is at converting energy from

one form to another.The amount of energy generated by PV cells is determined by the properties (such as intensity and wavelengths) of the available light as well as the cell's many performance factors.The band gap of PV semiconductors is an important feature that determines what wavelengths of light the material can absorb and convert to electrical energy. If the band gap of the semiconductor matches the wavelengths of light shining on the PV cell, the cell can efficiently use all of the available energy.

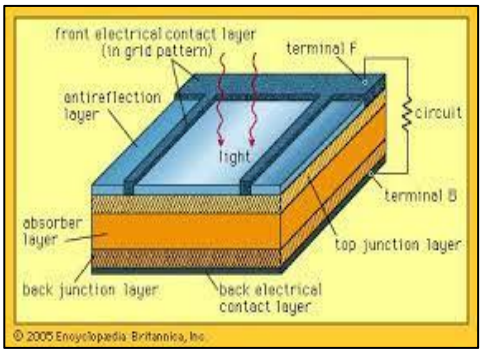

Fig : 1.3. Construction of Solar Cell

A photo-voltaic (PV) cell must have three basic characteristics in order to function:

1.Light absorption, resulting in either electron-hole or hole-electron pairs.

2.The separation of opposite-type charge carriers.

3. Separate carrier extraction to an external circuit[9].

1.3.2. TYPES OF SOLAR CELLS:

The solar cells are divided into three generations ,

I) First generation solar cells
II) Second generation solar cells
III) Third generation solar cells

Based on the materials used the generation of solar cells are further classified

First generation solar cells are classified into

I) Mono-crystalline Silicon PV
II) Poly-crystalline Silicon PV
III) Amorphous silicon PV

Second generation solar cells are classified into

I) Cadmium telluride (CdTe)
II) Copper indium gallium selenide (CIGS)
III) Dye sensitized solar cell (DSC)
IV) Organic solar cell
V) Amorphous solar cells

Third generation solar cells are classified into

I) Dye sensitized nanocrystalline TiO2 solar cells
II) Molecular OSC
III) Polymer solar cells

1.3.3 . FIRST GENERATION SOLAR CELLS:

Silicon solar cells are used in "first generation" panels. They are either cut from a block of silicon made up of several crystals or manufactured from a single silicon crystal (mono-crystalline).

(i)MONOCRYSTALLINE SOLAR CELLS:

Mono-crystalline solar panels are the purest, as they are built of mono-crystalline silicon. They come in a dark colour scheme with rounded edges. The high purity of silicon is due to the fact that this type of solar panel has the maximum efficiency of more than 20%.Mono-crystalline solar panels having the advantages of producing more power, taking up less space, and lasting longer. In comparison to other forms of solar panels, they are also quite costly. Another advantage is that they are less susceptible to high temperatures than poly-crystalline panels[10].

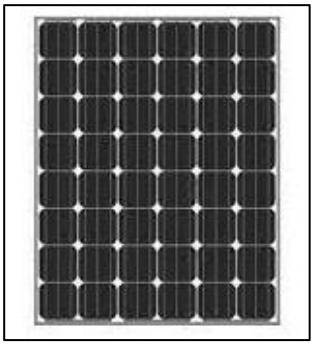

Fig.1.4:Monocrystalline solar cells

(ii)POLYCRYSTALLINE SOLAR CELLS:

Poly-crystalline solar panels have a distinct appearance from conventional panels. Squares are used in this form of solar panel, and the angles are not trimmed. This panel has a blue and speckled aspect to it.When opposed to mono-crystalline panels, these solar panels are made by melting raw silicon, which is a faster and less expensive technique.This is owing to a 15% reduction in efficiency, a reduction in space efficiency, and a shorter lifespan, even at reduced end prices, because they are more influenced by warmer temperatures. The space efficiency is slightly higher at a higher cost, but the power outputs are the same[10].

Fig.1.5: Polycrystalline solar cells

(iii)AMORPHOUS SILICON SOLAR CELLS:

The non-crystalline type of silicon is known as amorphous silicon (a-Si).Amorphous silicon can be deposited at extremely low temperatures, as low as 75 degrees Celsius, making it possible to deposit it on plastic. A single sequence of p-I-n layers makes up the cell structure in its most basic form. The low efficiency rate is owing in part to the Stabler-Wronski effect, which occurs within the first few hours after the panels are exposed to sunlight and causes an amorphous silicon panel's energy yield to drop from 10% to roughly 7%. The main benefit of amorphous silicon solar cells is that they have lower production costs, making them very cost competitive[9].

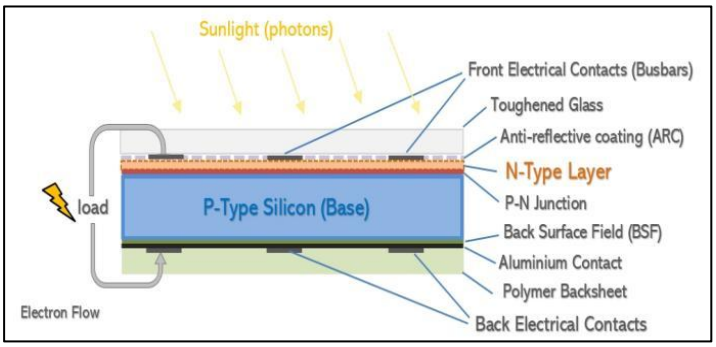

Fig.1.6: Internal structure of solar cells

1.3.4. SECOND GENERATION SOLAR CELLS:

Thin-film solar cells of the "second generation" are less expensive to manufacture than standard silicon solar cells since they need less ingredients.Thin-film PV cells are, as the name suggests, a type of thin-film solar cell technology that is physically thin and has been applied to photovoltaics. They are only somewhat less effective than other options. They do need a larger surface area to generate the same amount of heat a certain amount of power.

(i)CADMIUM TELLURIDE SOLAR CELLS:

Cadmium Telluride (CdTe) photovoltaics is a photo-voltaic (PV) technique that uses a thin semiconductor layer called cadmium telluride to collect and convert sunlight into electricity. Cadmium Telluride PV is the only thin film technology that is less expensive than crystalline silicon solar cells in multi-kilowatt systems. Cadmium is a toxic substance which on intake into the human body causes cancer. Tellurium is not toxic as cadmium but it is not present abudant in nature. Tellurium is a rare earth element found 1-5 parts per billion. The Tellurium of which telluride is the most common form is in short supply comparable to platinum in the anionic form in the Earth's crust, and it makes a considerable contribution to the module's price.

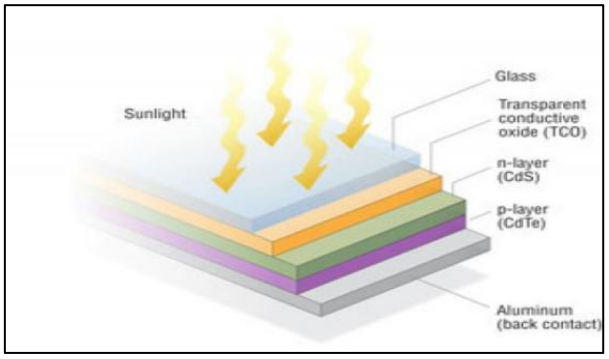

Fig.1.7: Internal structure of CdTe solar cells

(ii)COPPER INDIUM GALLIUM SELENIDE SOLAR CELLS:

Copper indium gallium selenide was also called as CIGS solar cells. A copper indium gallium selenide solar cell (or CIGS cell, often referred to as a CI(G)S or CIS cell) is a thin-film solar cell that converts sunlight into electricity. A thin layer of copper, indium, gallium, and selenide is deposited on glass or plastic backing, with electrodes on the front and back to collect current. Because the material has a high absorption coefficient and absorbs sunlight strongly, it necessitates a considerably thinner coating than other semiconductor materials.These technologies typically employ high-temperature deposition processes, with cells produced on glass providing the greatest results[9].

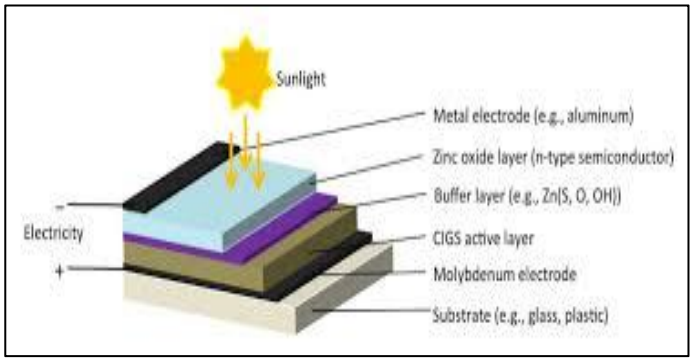

Fig.1.8: Internal structure of GIGS solar cells

1.3.5.. THIRD GENERATION SOLAR CELLS:

Third-generation technologies strive to improve the second-(thin-film generation's technologies) electrical performance while keeping production costs low. Third-generation solar cells, in general, are those that do not require the p-n junction seen in traditional semiconductor, silicon-based cells. Polymer solar cells, mono-crystalline solar cells, and dye-sensitized solar cells are among the third generation's prospective solar breakthroughs.

(i)DYE SENTISIZED SOLAR CELLS:

Dye-sensitized solar cells (DSSC), also known as dye-sensitized cells (DSC), are a type of third-generation photo-voltaic (solar) cell that transforms any visible light into electricity. Because of the way this new class of sophisticated solar cells replicates nature's absorption of light energy, it's been compared to artificial photosynthesis.This can generate electricity in a variety of light settings, both indoors and out, allowing users to convert both artificial and natural light into electricity.A photo electrochemical system is based on a semiconductor produced between a light-sensitized anode and an electrolyte. The DSSC has a number of appealing characteristics: it is simple to create using traditional roll-printing techniques, it is semi-flexible and semitransparent, allowing for a variety of applications not possible with glass-based systems, and most of the materials used are inexpensive. In actuality, removing a number of expensive components, notably platinum and ruthenium, has proven difficult, and the liquid electrolyte poses a severe obstacle to developing a cell appropriate for usage in all weather conditions.Although its conversion efficiency is lower than that of the finest thin-film cells, its price/performance ratio should be sufficient to allow it to compete with fossil fuel electricity generation by achieving grid parity.[09].

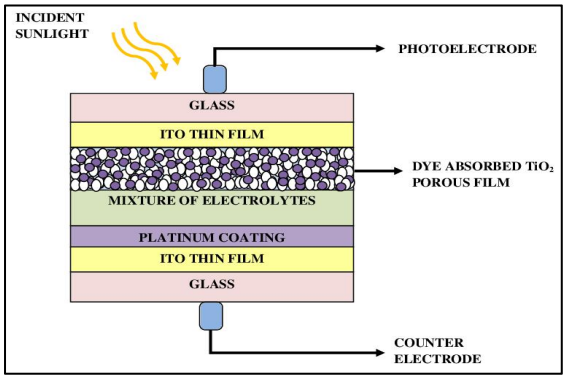

Fig.1.9:Dye sentisized solar cells

1.3.6.WORKING OF THE SOLAR CELLS:

Photo-voltaic (PV) cells Direct Current (DC) electricity can be generated by converting sunlight. Charge controllers control the power from solar panels, which can cause panel damage if the power is reversed back to the panels. When sunlight is not available, a battery system is used to store electric power (i.e. night). This system is linked to an inverter, which converts Direct Current (DC) to Alternating Current (AC).Solar radiation was directly converted into electricity by the cells. It is made up of a variety of semiconductor materials. This cell technology is used to create solar cells that are both inexpensive and efficient. When photons from sunlight are absorbed by the cell, electrons are knocked free from silicon atoms and drawn off by a grid of metal conductors, causing an electric direct current to flow. PV solar cells are made up of a variety of chemicals[11].

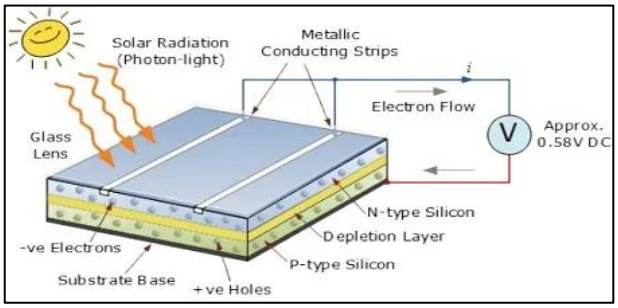

Fig.1.10: Schematic working diagram of solar cells

1.3.7.NEED FOR THE SOLAR CELLS:

1.The demand for low-maintenance, long-lasting electricity sources suitable for locations remote from both the main power grid and people, such as satellites, remote site water pumping, outback telecommunications stations, and lighthouses.

2.The demand for low-cost power supplies for people living in areas far from the main power grid, such as Aboriginal settlements, outback sheep and cattle stations, and some grid-connected home sites.

3.The need for non-polluting, silent electricity; e.g., tourist sites, caravans, and campers.

4. The requirement for a portable and adaptable source of small amounts of power, such as calculators, watches, light metres, and cameras[10].

1.3.8.APPLICATIONS OF SOLAR CELLS:

1.In Power Plants: Nonrenewable energy sources are used in conventional power plants to boil water and form a stream so that turbines can rotate and water can produce electricity. However, with the use of solar energy, the heat of the sun can boil that water, resulting in steam and rotating turbines. Panels, photoelectric technologies, and thermoelectric technologies, among other things, are used to convert sunlight into electricity.

2.In residential use: Solar energy is also becoming more common in homes. Residential appliances can run well on energy from the sun electricity. Apart from that, solar energy is used to power solar heaters that provide hot water to homes. Energy is captured and accumulated on batteries by photo-voltaic cells installed on the roof of the house, which can then be used end-to-end day at home for various purposes. Home users are reducing their energy consumption in this way.

3.**In commercial use:** Glass PV systems or any other type of solar panel can be noticed on the roofs of various buildings.These panels can be used to provide dependable electricity to various offices and other parts of the building. These panels collect solar energy from the sun, converting it into electricity, and allow companies to use their own power for a number of purposes.

4. In solar lighting: On the roofs of various buildings, glass Photovoltaic systems or any other type of solar panel can be seen. These panels can be used to provide consistent power to various offices and other areas of the building. These panels capture sunlight and convert it to electricity, allowing businesses to use their own power for a variety of applications.

5. In solar cars: It's an electric vehicle that gets its power from the sun or solar energy. This car has solar panels that absorb sunlight and convert it into electrical energy. This energy will be stored in the car's batteries, allowing us to drive these vehicles at night as well[12].

Fig.1.11: Various applications of solar cells

1.4.TRANSPARENT CONDUCTIVE OXIDES:

TCO's are binary or ternary compounds that contain one or two metallic elements and are optically transparent and electrically conducting. Because of their large optical band gap (Eg) of greater than 3 eV, their resistivity could be as low as 10 -4 cm, and their extinction coefficient k in the optical visible range (VIS) could be lower than 0.0001. This unusual combination of conductivity and transparency is usually impossible to achieve in intrinsically stoichiometric oxides; however, it can be achieved by producing them with a non-stoichiometric composition or by adding appropriate dopants. Thin CdO films with such properties were discovered by Badeker. Thin films of ZnO, SnO_2, In2O3, and their alloys were later recognised as TCOs by Haacke. Doping these oxides improved their electrical conductivity while not affecting their optical transmission.In specific, ITO is widely used.Depositing p-type TCO films is a recent effort to develop novel TCO materials. The majority of TCO materials are n-type semiconductors, but solid laser development requires p-type TCO materials. ZnO:Mg, ZnO:N, ZnO:In, NiO, NiO:Li, CuAlO2, Cu2SrO2, and CuGaO2 thin films are examples of p-type TCOs. These materials have yet to be used in real-world applications.

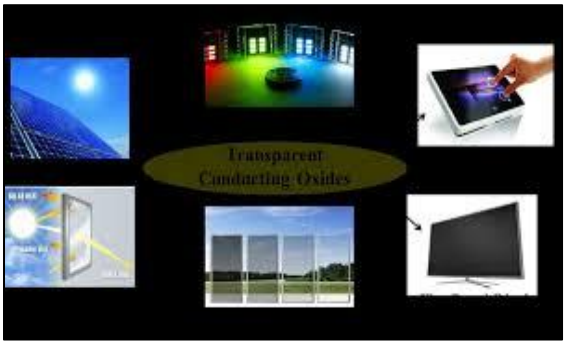

Fig.1.12: Applications of TCO

1.4.1. APPLICATIONS:

(i) Transparent electrodes for flat panel displays;

(ii) transparent electrodes for photovoltaic cells;

(iii) low emissivity windows;

(iv) window defrosters;

(v) transparent thin films transistors;

(vi) light emitting diodes; and

(vii) semiconductor lasers are some of the current and potential applications of TCO thin films. Because TCO thin films' utility is determined by both their optical and electrical properties, both should be considered along with environmental stability, abrasion resistance, electron work function, and compatibility with the substrate and other components of a device, as appropriate for the application. The availability of raw materials and the cost of the deposition method are also important considerations when selecting the best TCO material.

1.4.2. PROPERTIES OF TCO:

(I)ELECTRICAL PROPERTIES:

TCOs are semiconducting oxides with a wide band gap (Eg) and conductivities ranging from 10^2 to 1.2×10^6 (S). Doping, either by oxygen vacancies or by extrinsic dopants, is responsible for the conductivity. In the absence of doping, these oxides become excellent insulators, with a dielectric constant of $\rho > 10^{10}$ Ω-cm. TCOs are mostly n-type semiconductors. The mobility of electrons in the conduction band and their mobility determine the electrical conductivity of n-type TCO thin films: $\rho=\mu ne$, where is μ the electron mobility, n is its density, is σ conductivity, and e is the electron charge.

(II)OPTICAL PROPERTIES:

Effective TCO thin films should have a very low absorption coefficient in the near UV-VIS-NIR region, in addition to high conductivity (10^6 S). Photons with an energy greater than Eg are absorbed, limiting transmission in the near UV. The NIR region has a second transmission edge, owing to reflection at the plasma frequency. In the UV-VIS-NIR region, a wide band gap TCO should not absorb photons in the transmission "window." However, no "ideal" TCOs thin films exist, and even if they could be deposited, reflection and interference would affect transmission. As a result, achieving

100 percent transparency over a large area is impossible.The optical parameters of the TCO film, as well as the optical properties of the substrate, influence the width of the VIS transmission window of a TCO film with thickness deposited on a transparent substrate[13].

1.5.TITANIUM ISOPROPOXIDE:

Titanium isopropoxide, also commonly referred to as titanium tetraisopropoxide or TTIP, is a chemical compound with the formula Ti{OCH(CH3)2}4. This alkoxide of titanium(IV) is used in organic synthesis and materials science. It is a diamagnetic tetrahedral molecule. Titanium isopropoxide is a component of the Sharpless epoxidation, a method for the synthesis of chiral epoxides.The structures of the titanium alkoxides are often complex. Crystalline titanium methoxide is tetrameric with the molecular formula $Ti_4(OCH_3)_{16}$. Alkoxides derived from bulky alcohols such as isopropyl alcohol have less aggregation. Titanium isopropoxide is a monomer mainly in non-polar solvents[33].

Fig.1.13.Titanium isopropoxide

✧ ***TITANIUM TYPES:***

Titanium oxide (TiO_2) is an important material which has a lot of properties and applications. They are of two types rutile and anatase. The anatase TiO_2 is colorless and it is a optically negative.

(I)RUTILE TITANIUM:

The rutile TiO_2 is dark red in appearance and it is optically positive. Rutile titanium has a high stability and has a tetragonal unit structure.

PROPERTIES OF RUTILE TITANIUM:

i) Greater dispersion
ii) Higher birefringence
iii) Greater refractive index

Applications :

I) It is used for the manufacture of metallic titanium and titanium dioxide pigments.

II) It is used for the manufacturing of plastics, paper and paints.

III) It has the ability to absorb UV rays and transparent to visible light.

(II) ANATASE TITANIUM:

It is a colorless or yellow color. Anatase titanium contains a lot of impurities which makes it dark. The structure of anatase TiO_2 is tetragonal. Their appearance is metallic and they are used for the manufacture of semiconductors.

TABLE 1.1: DIFFERENCES BETWEEN RUTILE AND ANATASE TITANIUM:

RUTILE	ANATASE
It is dark red in color	It is colorless to blue
It is basically a dark red in color and finely pulverized rutile titanium shows a bright white color	It is dark in colors in impurities and in the pure form it is colorless/white
Rutile TiO_2 is optically positive	Anatase TiO_2 is optically negative
The UV absorption is great in Rutile	The UV absorption is low in Anatase
The hardness of the rutile TiO_2 is great	The hardness of anatase TiO_2 is not that hard
The density is high	The density is low

1.6.MAGNESIUM ACETATE TETRAHYDRATE:

$Mg(C_2H_3O_2)_2$ is the chemical formula for anhydrous magnesium acetate, and $Mg(CH_3COO)_2 \cdot 4H_2O$ is the chemical formula for hydrated magnesium acetate tetrahydrate. Magnesium's oxidation state is 2+ in this compound. The magnesium salt of acetic acid is commonly known as magnesium acetate. It is deliquescent and decomposes into magnesium oxide when heated. In biological reactions, magnesium acetate is a common source of magnesium.Magnesium acetate has the appearance of white hygroscopic crystals. It has a similar odour to acetic acid and is soluble when placed in water (H_2O). Its pH level will be on the alkaline side of neutral when it is in the form of an aqueous solution.Magnesium acetate is a very safe compound to work with, with a health hazard rating of zero (0). However, we

should always use gloves and safety goggles when dealing with it. Irritation will occur if it gets into the eyes or on the skin, or if it is ingested or inhaled[15].

Fig.1.14:Magnesium acetate

TABLE.1.2:COMPARING THE PROPERTIES OF MAGNESIUM AND TITANIUM:

S.No.	***PROPERTIES OF MAGNESIUM***		***PROPERTIES OF TITANIUM***	
1	Atomic number	22	Atomic number	12
2	Atomic mass	47.90 g.mol -1	Atomic mass	24.305 g/mol
3	Electronegativity according to Pauling	1.5	Electronegativity according to Pauling	1.2
4	Density	4.51 g.cm-3 at 20°C	Density	1.74 $g.cm^{-3}$ at 20°C
5	Melting point	1660 °C	Melting point	650°C
6	Boiling point	3287 °C	Boiling point	1107°C
7	Vanderwaals radius	0.147 nm	Vanderwaals radius	0.16nm
8	Ionic radius	0.09 nm (+2) ; 0.068 nm (+4)	Ionic radius	0.065nm
9	Isotopes	8	Isotopes	5
10	Electronic shell	[Ar] 3d1 4s2	Electronic shell	[Ne] $3s^2$

11	Energy of first ionisation	658 kJ.mol -1	Energy of first ionisation	737.5 $kJ.mol^{-1}$
12	Energy of second ionisation	1310 kJ.mol -1	Energy of second ionisation	1450 $kJ.mol^{-1}$
13	Energy of third ionisation	2652 kJ.mol -1	Energy of third ionisation	-
14	Energy of fourth ionisation	4175 kJ.mol -1	Energy of fourth ionisation	-
15	Discovered by	Sir Humphrey Davy in 1808	Discovered by	Sir Humphery Davy in 1808

PROPERTIES OF PHOTOANODE MATERIALS:

1.7.MAGNESIUM DOPED TITANIUM :

1.7.1.PROPERTIES OF TITANIUM:

Photon absorption and electrical conductivity are both low in TiO_2. Because anatase TiO_2 has a band-gap value of 3.3 eV, it is photoactive in the ultraviolet (UV) range of electromagnetic radiation, which accounts for only 5% of solar radiation. As a result, synthesising TiO_2 thin films photoactive in the visible range of the electromagnetic spectrum, which accounts for nearly 40% of solar radiation, is preferable. Doping metal into TiO_2 is one way to improve its photoabsorption and conductivity, reducing hysteresis and suppressing charge accumulation[2].For its high photocatalytic activity, nontoxic property, chemical stability, and highest oxidation rate of many photoactive metal oxides investigated, TiO_2 has sparked a lot of research. TiO_2 can break down a variety of organic, inorganic, and toxic pollutants.TiO_2 has a high bandgap energy (3.2 eV), but it only accounts for 4-5 percent of the total solar spectrum. As a result, the use of visible light is limited. Second, TiO_2 particles have a low photoquantum efficiency due to the high rate of electron-hole recombination[16].

1.7.2.ABSORPTION PROPERTIES OF MAGNESIUM DOPED TITANIUM:

Mg-doped TiO_2 polyscales and pure TiO_2 both have a strong absorption band at 380–420 and 387 nm, respectively, which is near the UV region. Broad absorption edges were observed in Mg-doped TiO_2 polyscales at 398 nm, which is within the visible spectrum of light. When compared to pure TiO_2, the optical absorption edges of Mg-doped TiO_2 polyscales showed significantly shifted edges toward visible spectrum of light. The decrease in energy level in the conduction band, as a result of the shift in

the absorption edge to smaller photon energy, implies a narrowing band gap energy.Band-tuning of Mg-doped TiO_2 polyscales is clearly indicated by this shift in the absorption edge towards the nearvisible region.In the destruction of industrial dyes, Mg-doped TiO_2 polyscales showed a higher photocatalytic degradation efficiency than pure TiO_2 [17].

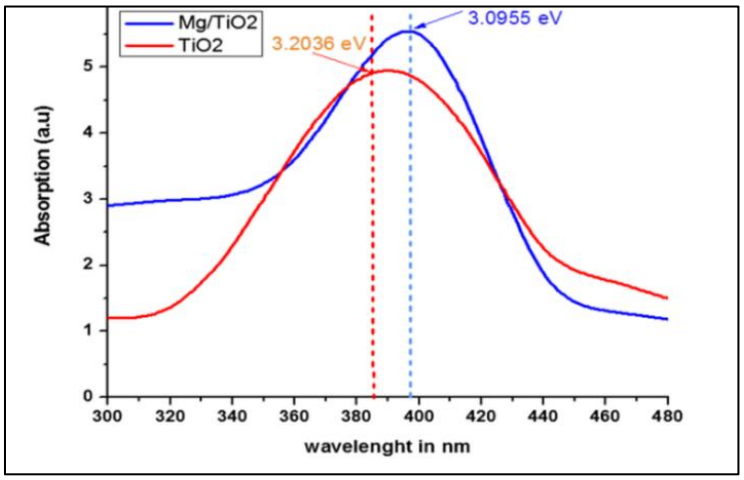

Fig.1.15.Graph marked between wavelength and absorption[17]

1.8.TITANIUM AS A HOLE BLOCKING LAYER:

Introducing Mg into the perovskite solar cells' compact TiO_2 HBL, which can provide better hole-blocking effect while still allowing electron transfer from perovskite to TiO_2. The perovskite solar cells employing Controlled cells using Mg-doped TiO_2 HBLs outperform the Mg-doped TiO_2 HBLs. Because of the following factors, TiO_2 HBLs exist:

(1) Mg-doped TiO_2 has a higher CBM and a lower VBM, which are more compatible. with the energy bands of the porous TiO_2 and $CH_3NH_3PbI_3$, As a result, cells with higher V_{oc} and fill factor values are produced.

(2) Mg-doped TiO_2 has a larger band gap and better optical transmission properties, resulting in larger cells Jsc's values.

(3) Mg-doped TiO_2 has a much longer electron life time and a lower contact resistance, indicating that there is less electron and hole recombination, which improves both the Voc and the Jsc. Creating an optimised Mg-doped TiO_2 based device with a 100 mV increase in Voc over the pure TiO_2 based device, as well as improvements in J_{sc} and FF.

Adding magnesium acetate tetrahydrate to a commonly used compact TiO_2 solution, whose main component was tetrabutyl titanate in ethanol. The tetrabutyl titanate would hydrolyze immediately after a small amount of magnesium acetate tetrahydrate was added, resulting in a compact film with

pores and agglomerated particles. As a result, $TiCl_4$ was used because it hydrolyzes less.The optical absorption edges of Mg-doped TiO_2 films shift to a shorter wavelength range, resulting in improved transmission, particularly in the short wavelength region.The energy band broadens when Mg is added to TiO_2, shifting the bottom of the conduction band up and the top of the valence band down.Mg-doping benefits the IPCE primarily at short wavelengths, which should be due to improved light transmission in the corresponding wavelength range and improved cell charge transportation. A thin layer of magnesium oxide and magnesium hydroxide formed on the HBL's surface, which suppressed recombination at the compact TiO_2 surface, resulting in a further increase in V_{oc}[18].Because of its optimal band gap alignment with perovskite, low cost, and environmentally stable properties, TiO_2 is a commonly used ETL material[2].

1.9.ABSORPTION OF Mg DOPED TiO_2:

The absorption spectra of undoped and Mg doped TiO_2 show that Mg doping causes higher absorption and a red shift in the absorption range. The increased absorption on doing Mg is due to a decrease in band gap and increase in Fermi energy, making it easier for electrons to jump from the valence to conduction band[2]. When compared to undoped TiO_2, which can only be excited in less available UV light, magnesium doping causes better separation of electrons and holes on the modified TiO_2 surface, allowing more efficient channelling of the produced electrons into useful redox reactions, thus enhancing DDVP degradation in the presence of visible light[20].

1.10.TITANIUM WITH OTHER DOPANTS:

1.10.1.WITH CALCIUM:

The elemental composition of Ca-doped TiO_2 thin films reveals that the concentration of Ca dopant is slightly higher or lower than the initial evaporation material, but that the concentration of calcium dopant in the Ca-doped thin films is gradually increasing by a factor of two increasing the dopant content of the starting powder. This minor discrepancy can occur as a result of various factors. Ca, Ti, and their oxides evaporation rates. This could also be due to the fact that CaO (2613) melts at different temperatures. TiO_2 (1843 °C) and TiO_2 (1843 °C). When titanium dioxide is heated, calcium oxide sinks to the bottom of the crucible melted. During the deposition, this gives the CaO concentration gradient through the depth of the initial material process.The electron conductivity of Ca-doped titanium dioxide is mixed electronic protonic conductivity, with the electron conductivity decreasing as the Ca dopants concentration increases. The total conductivity is affected by the size of the crystallytes and decreases as the size of the crystallytes increases. Ca-doping reduced the total conductivity of the formed thin films, according to impedance measurements. Under wet reducing

conditions, the total conductivity ranges from 2.7 S/cm in pure TiO2 to 4 10^{-4} S/cm in 2.5 percent Ca doped TiO_2 at 800 °C, and from 5.4 10^{-4} S/cm in pure TiO2 to 3.4 10^{-5} S/cm in 0.5 percent Ca doped TiO_2 at 800 °C. The conductivity of a reducing atmosphere is higher than that of an oxidising atmosphere[19].

1.10.2.WITH ZINC:

The powders made from zinc sulphate have $ZnTiO_3$ and $ZnSO_4$ 3Zn $(OH)_2$ diffraction peaks.None of the peaks for titanium compound can be found in any XRD patterns. This could be due to the fact that titanium molecules occupy some sites that were previously only accessible to zinc molecules, or because titanium molecules are amorphous. Furthermore, titanium-doped ZnO powders synthesised from zinc nitrate and zinc chloride have sharper peaks and a narrower half peak width than others.Titanium doped ZnO powders, which were synthesised from zinc acetate, zinc nitrate, and zinc chloride, have absorption edges of more than 400 nm. However, the powders' absorption edge wavelength is less than 400 nm. The absorption edge of zincite ZnO is 387 nm, demonstrating that the powders' absorption edge shift is caused by particle size and crystal structure. The particle size of the titanium doped ZnO powders synthesised from zinc acetate is smaller than the others, enhancing their quantum size effect.The titanium-doped ZnO powders synthesised from zinc acetate and zinc nitrate have the same absorption edge wavelength, but the particle size of the powders synthesised from zinc nitrate is larger than that of the powders synthesised from zinc acetate. The reason for this could be that powders made from zinc nitrate have a better doping effect than powders made from zinc acetate. Furthermore, the powders synthesised from zinc chloride have a longer absorption edge wavelength than the others. This is due to the fact that some particles are smaller than others. Furthermore, when zinc sulphate is used as a zinc salt, the samples' absorption edge is lower than the other. It could be for one of two reasons.The first is that there are crystals of ZnO, $ZnTiO_3$, and $ZnSO_4$ 3Zn $(OH)_2$, and composite semiconductors cannot reduce the band gap. Due to irregular powders, they have a poor quantum size effect[21].

1.10.3.WITH NIOBIUM:

Because of its similar radius to titanium, niobium metal (Nb) is a good candidate as a doping material for titanium oxide electron transport materials.Nb doping could improve conductivity and mobility while simultaneously lowering the trap-state density of TiO_2 ETLs for PSCs.In PSCs based on Nb-doped TiO_2, a relatively high-temperature (150 °C) treatment was required, and large hysteresis was still observed.a simple one-step, in situ, low-temperature (70 °C) strategy for producing hysteresis-free PSCs with a single Nb:TiO_2 compactmesoporous layer that serves as both scaffold and ETL. A compact TiO_2 bottom with nano-pin morphology on the surface of the Nb:TiO_2 layer can be used as a scaffold.

Due to the collaborative effect of the increased interface surface area caused by nano-pin morphology on the surface and the improved carrier transportation rate due to the presence of Nb, the hysteresis index decreased significantly from 24.39 percent for the PSC based on bare TiO_2 to 3.19 percent for the PSC based on 2 percent Nb:TiO_2 layer. The PSCs were able to achieve a remarkable PCE of 19.7% thanks to the high-quality mesoporous layer.This research suggests a scalable and cost-effective method for achieving hysteresis-free and high-efficiency PSCs at low temperatures.The bare TiO_2 has a much smoother surface than the compact TiO_2 layers in planar PSCs, which is a typical morphology of compact TiO_2 layers in planar PSCs. However, a nano-pin texture is visible on the compact bottom of TiO_2 with 2% Nb doped. The nano-length pin's was determined to be 50 20 nm. This indicates that the Nb:TiO_2 layer has a compact TiO_2 layer on the surface with a nano-pin morphology, which is classified as a mesoporous layer. As a result, the PSC's in situ formed Nb:TiO_2 compact-mesoporous layer, which was created in a single step, serves as both a scaffold and an ETL.The main absorption edge of bare TiO_2 and Nb-doped TiO_2 is observed at wavelengths of 300–350 nm. Nb doped TiO_2's absorption curve almost completely overlaps that of bare TiO_2. Using the Tauc equations, the energy bandgap (Eg) can be calculated based on the absorption spectra. The Nb doped TiO_2-based device's hysteresis suppression is caused by the conductance increasing and the nano-pin morphology forming. Charge accumulation at the ETL/perovskite interface caused by interfacial capacitance would be reduced, resulting in a hysteresis-free character[22].

1.10.4.WITH SILVER(Ag):

Ag doping lowers the band gap energy, which is the energy required to move an excited electron from the valence to the conduction band. The higher the Ag content, the higher the absorption of wavelengths.In the literature, it has been discovered that $(TiO_2)_{1-x}(Ag)_x$ has direct band gaps, with the band gap values varying depending on the preparation parameters and conditions.For all films, it can be seen that (E_g) is decreasing as doping levels rise. Ag doping resulted in increased levels of localised near valence band and conduction band, which are ready to receive electrons and generate tails in the optical energy gap, which are working to reduce the energy gap, or can be attributed to the increased size of particles in the films, according to wavelength absorption analysis. Not only did Ag doping reduce band gap energy, but it also prevented charge recombination between electron-hole pairs.Due to the increased refractive index, doping TiO_2 with noble metal Ag increases the real and imaginary parts of dielectric constants.The effect of increasing the doping TiO_2 of Ag concentration on the extinction coefficient values is due to increased absorption, which leads to a decrease in defects or deep tails, thus increasing the extinction coefficient values[23].

1.10.5.WITH CADMIUM OXIDE:

Cadmium oxide (CdO) is a desirable II-VI group semiconductor with high transparency and suitability for optoelectronic applications. As a result of its practical features such as optical and electrical properties, CdO is used in a variety of applications such as photovoltaics, gas sensors, diodes, and photodevices. It has a direct bandgap of 2.2eV, allowing it to absorb the majority of the solar spectrum and thus achieve better results in optoelectronic applications.However, there is a limitation in the case of TiO_2 because it has a large band gap of 3.2 eV, which causes it to absorb UV radiation from the sun.Although isolated CdO and TiO_2 have better properties, compositions of CdO and TiO_2 are more suitable in optical and electrical applications and make it easier to overcome some of the limitations imposed by isolated CdO or TiO_2, such as UV absorption, fast recombination of electron hole pairs, charge accumulate, particle aggregation, and so on. In photovoltaic applications, the composite form of CdO and TiO_2 has a significant effect, and the photo conversion efficiency (PCE) improves at the same time. This occurs as a result of TiO_2 reacting with CdO, forming a new impurity level in the forbidden band. Cd^{+2} reacts with Ti^{+4} to increase charge separation and bring it into the visible spectrum, allowing opto-electronic applications to be performed.Because Ti^{+4} has a higher stability and is found at interstitial or substitutional sites, it has a donor tendency when associated with oxygen vacancies, whereas oxygen interstitials and Cd^{+2} vacancies have an accepter tendency.The main advantages of both CdO and TiO_2 are that they have negative charge mobility due to inhabit defects and are able to place composition layers on p-Si, resulting in the formation of a p-n junction. When light strikes the junction, photon energy is transferred to silicon electrons, and the energy gained is sufficient to free electrons from their parent silicon atom. Inside the n-type composition of CdO:TiO_2 layers, free electrons move and gather. The terminals are connected to the outside circuit, and the electric current is produced by electrons moving from n-type to p-type through cathodes and the outer circuit.Within the wavelength range of 300 nm to 800 nm, transmittance spectra of CdO:TiO_2 thin films were obtained.The conductivity of CdO thin films was improved while the toxicity of CdO was reduced by adding TiO_2.With an exposure area of 1.80 x 1.80 cm2, the fill factor and efficiency were found to be 0.53 and 3.23 percent, respectively[24].

1.11.CONCLUSION:

Dopants of titanium is used both as a electron transport layer and hole blocking layer. Doping of Magnesium into Titanium increases the photocatalytic degradation efficieny. Titanium are doped with various elements with different concentrations. Doping magnesium causes better separation of electron and holes on the surface of TiO_2 allowing more efficient channeling of the produced electrons into useful redox reaction. Doping the Mg into TiO_2 causes a shift in the absorption band from UV to Visible region. Among all the dopants of titanium noebium has the highest efficiency of all.

Conductivity and the activation energy depends on the magnesium concentration and the temperature. Though the titanium is doped with many other dopants here in this project we take the magnesium and study the characterisation when it is doped as $MgTiO_2$. Here we have coated electrodes[electrode-1(ZTO-1-Mg/TiO_2), electrode-2(ZTO-2-Mg/TiO_2), electrode-3(TO 1-Mg/TiO_2), electrode-4(TO 2-Mg/TiO_2) and electrode-5(FTO-$MgTiO_2$)] different TCO's and they were analysed and discussed.

CHAPTER-2

REVIEW OF LITERATURE

2.1.INTRODUCTION:

The term "review of literature" refers to all previous research and scholarly work on the subject. The overall study issues in many articles connected to solar cells, Mg doped TiO_2 materials, and their approaches are discussed in this chapter. The review of literature elucidates the topic in greater detail.information on the subject The synthesis of the available literature is called a literature review.Mg doped TiO_2 and solar cells were taken into consideration. Their previous findings and research projects are well-known It provides a wealth of information and ideas for completing the project.

2.2.REVIEW OF LITERATURE:

1. Sameeksha Sharma et al. (2021): This paper is based on changes in the structural, optical, electrical, and dielectric properties of the perovskite solar cell (PSC) electron transport layer (ETL), . H. Impurities of magnesium (Mg), zinc (Zn), and silver (Ag) are added to titanium dioxide (TiO_2) by the sol-gel method. The modified parameters are studied using electrical and dielectric measurements using X-ray diffraction (XRD), UVVisible (UVVis) spectroscopy, and two-probe methods. This result shows modified $MgTiO_2$, $ZnTiO_2$, $AgTiO_2$, etc. with improved transmittance (T), decreased refractive index (n), quenching factor (k), Urbach energy (EU), increased DC conductivity, etc. Achieved. , Dielectric constant (ϵ) and AC conductivity. The conductivity of modified TiO_2 follows the order $AgTiO_2$> $ZnTiO_2$> $MgTiO_2$> TiO_2. The prepared samples are used in the manufacture of PSC devices, and the efficiency gains that follow in the same order as conductivity suggest the idea of successfully doping ETL with in solar cell applications[49].

2. M.Stefan et al. (2021): $CoFe_2O_4$ / TiO_2: Tb composite nanoparticles were prepared by a two-step chemical pathway. The composite material was characterized using X-ray diffraction, transmission electron microscopy, X-ray and UV photoelectron spectroscopy, FTIR, Raman, and UV-Vis spectroscopy. Polarization spin transfer occurs at the interface between the cobalt ferrite and the TiO_2 conduction band. As a result of , the magnetic moment of the oxygen vacancies of TiO_2 is (iron) magnetically ordered. The sublattice of the magnetic moment of the Tb ion can indicate either a "ferro" or "antiferro" coupling, depending on the concentration of the dopant. The magnetic semiconductor intensifies the optical absorption in the visible. There is a bandtoband absorption assisted by

singleoccupied oxygen vacancies coupled to some local crystal lattice relaxations. The lifetime of the photoexcited electrons in the conduction band increases due to their coupling with magnetically ordered interface transferred states. Also, the trapping of electrons into multiplet states of Tb^{3+} reduces the recombination rate. The photocatalytic efficiency of the magnetically ordered titania increases with respect to bare TiO_2. The reactive oxygen species produced at the solid–liquid interface of TiO_2 were identified by Electron Spin Resonance coupled with spintrapping technique. The results were correlated to the presence of the magnetic order inside the titania[50].

3. Simon Saint Andre et al. (2021) : In this the results of the optimization of antireflection films of TiO_2 nanotubes on GaAs solar cells, non encapsulated and encapsulated, are presented. The ARC forms a bilayer of porous TiO_2 over a dense bottom. The films were prepared on Si and GaAs substrates via a versatile electrochemical anodization process which produces films with good optical performance. The thicknesses and porosity of the ARC were optimized numerically with a method based on maximizing the short circuit current. Using experimental indices, the minimum R_w was 1.81% for the nonencapsulated case. For the encapsulated package, the minimum R_w was 2.34%, and the porosity of the top layer was adjusted in addition to the thickness. Simulations of GaAs solar cells showed a J_{sc} increase of 43.6% with no encapsulation and 36.7% with encapsulation with the addition of optimized ARC[51].

4.Wei Huang et al. (2021) : Titanium and tungsten co doped indium oxide (IWTO) films are deposited via low damage reactive plasma deposition technique at room temperature (RT) and heating temperature (HT). The effects of oxygen flow rates (FO_2) on the structural, optical and electrical properties of the IWTO films are investigated after air annealing. X-ray diffraction and scanning electron microscopy results show that the IWTO films are polycrystalline structure exhibiting a preferred (222) crystal plane orientation. As FO_2 increases from 10 sccm to 80 sccm, carrier concentration decreases by an order of magnitude for both RT and HT condition, while carrier mobility first increases and then decreases. It is noteworthy that films fabricated at HT show highest mobility (92.1 $cm^2\ V^{-1}\ s^{-1}$) and lowest resistivity (2.13 × 10− 4 Ω cm) due to better crystallinity and hence decreased grain boundary scattering. In addition, the average transmittance of IWTO film exceeds 89.5% in the wavelength range of 400-1200 nm. Finally, for silicon heterojunction solar cells, the high efficiency of 4.444 (at open circuit voltage (Voc) 0.746 V), the short circuit current density (J_{sc}) of 38.7 mA cm-2 and the curb factor (FF) of 82.9%) Achieved by the application of high performance IWTO film[52].

5.Seyed Masoud Parsa et al. (2021) : The use of nanoparticles in solar thermal desalination is a new approach to improving system performance. The use of black nanoparticles in solar stills has been used

by some researchers, but the number of studies related to this is limited. In all previous studies, researchers typically used a single type of nanoparticles. Here in this study, 0.1 wt% silver (Ag), gold (Au), and titanium dioxide (TiO_2) were used in three double tilt solar stills. It examines the performance of energy, energy, economy, energy economy, environmental economy, CO_2 reduction, and energy matrix systems. Results show that the thermal efficiency of Ag-based solar systems is calculated to be about 33.68%. This represents a improvement of about 7.6%, 20.7% and 38.2% compared to Au, TiO_2, and traditional systems, while the overall energy efficiency is 2.34% of the Ag-based system. , About 7.3%, 32% and 70.5% higher than the system mentioned above. Energy and energy-based energy results were obtained with Ag, TiO_2, conventional and Au-based solar stills, from highs to lows of . In addition, Economic Assessment showed that the lowest and highest distilled water costs of $ 0.0065 / $l.m^{-2}$ and $ 0.0289 / $l.m^{-2}$ were generated by Ag-based and Au-based solar stills. CO_2 reduction rates for Ag, Au, TiO_2, and traditional systems are calculated to be approximately 10.82, 10.02, 8.87, and 7.7 t / year, respectively. The energy recovery time (EPBT) for all systems was less than 3 years. We can conclude that the use of silver nanoparticles is the most effective particle in terms of improvement amount and cost, but gold nanoparticles are expensive and suitable for use in Solar Still not[53].

6.Daniel Dorow Gerspach et al. (2021) : Highly conductive TiO_2 movies with special Nb doping levels (as much as five at%) have been prepared through reactive DC magnetron sputtering beneathneath specific manipulate of the oxygen partial stress. They have been deposited on unheated substrates, protected with a protecting Si_3N_4 layer, and subsequently annealed at 300 ℃. The doping performance of Nb is more than 90%. Conductivity is a most for a partially oxidized goal withinside the transition range. The satisfactory movies show off a resistivity of 630 μΩ cm and a mobility of 7.6 cm^2/Vs blended with a excessive transparency above 70%. Comparing the behavior of undoped and Nb-containing movies, intrinsic limits of the conductivity withinside the TiO_{2-x}:Nb system will be observed, and a constant version explaining those findings is presented. The conductivity is limited—through lowering electron density because of Nb oxidation—through growing incorporation formation of Nb_2O_5 clusters as scattering facilities with growing oxygen partial stress and Nb concentration, through a transition from the crystalline to the amorphous country of the movies beneathneath a crucial oxygen partial stress[54].

7.S.C. Vella Durai et al. (2021) : This article describes a new synthesis for the preparation of titanium dioxide (TiO_2) nanoparticles by the sol-gel process using titanium tetraisopropoxide as the titanium source. The synthesized nanoparticles were analyzed using many measurements such as X-ray diffraction (XRD), HRTEM, absorption UV spectroscopy, FTIR, and AC impedance spectroscopy. Using X-ray peaks, crystallite size and lattice strain were calculated according to the Williamson-Hall method. The crystallite size calculated from X-ray diffraction using Scherrer's equation indicates a size

of approximately and cannot be used for measurement. It was found that the TiO_2 nanoparticles have a tetragonal structure with a crystal size of about 12 nm. Particle size was confirmed by HRTEM images. Optical Study of Nanoparticles The response of showed that the possible visible absorption peaks of TiO_2 nanoparticles were at 323 nm. Describes the bandgap energy (Eg) of TiO_2 nanoparticles calculated from the UV-visible absorption spectrum, with a bandgap of 3.14eV. The FTIR spectrum showed the vibration band of the TiO network. The AC conduction properties of TiO_2 nanoparticles have been studied in the 1-8 MHz frequency range at various temperatures. The conductivity of the TiO_2 nanoparticles was found to be constant over the low angular frequency range. Dielectric parameters were analyzed at various temperatures and frequencies[55].

8. Zafar Arshad et al. (2021): Perovskite solar cells (PSCs) are rapidly emerging as efficient solar cells due to the efficient photovoltaic and physiochemical properties. Ideally, the absorber layer in PSCs is sandwiched between highly conductive electron transport layer (ETL) and highly stable hole transport layer (HTL). The interfaces between these layers highly affect the performance of PSCs. In this study Magnesium (Mg) doped TiO_2 based ETL is systematically investigated to enhance the optical and morphological properties of the layer and the interface. It was observed that with Mg doping in mesoporous TiO_2, morphology of TiO_2 based ETL film was significantly improved thereby providing an interface for the growth of absorber layer. Optoelectronic studies suggested that band gap was effectively reduced with the addition of Mg and absorption range was also enhanced. Electrical analysis revealed that Mg-doped TiO 2-based ETLs showed improved conductivity and sheet support mobility compared to undoped films. Thermal studies have shown the production of thermally stable ETL materials for PSCs. In addition, a current density voltage (JV) measurement showed a more than double increase in photovoltaic efficiency from 3 wt% Mg[2].

9.Ibrahim Dundar et al. (2020) : A thin TiO_2 film was deposited from the solution by ultrasonic spray pyrolysis. At concentrations of 0.1 and 0.2M. Sedimentation temperature is set to 350 ° C, All samples were tempered in air at 500 ° C for 1 hour. The thickness of the TiO_2 film has been changed By varying the number of spray cycles from 1 to 21, in the range of 50 to about 800 nm Solution concentration. The result is that the average crystallite size of the anatase structure is Surface roughness and light absorption increased with film thickness. Movie effect The thickness of photocatalytic activity was investigated using photodegradation of stearic acid. Acid under UVA irradiation. Optimal thickness of TiO_2 film produced by ultrasonic spraying Pyrolysis in photocatalytic self-cleaning applications ranges from 170 to 230 nm, showing approximately 2.6 times higher photocatalytic self-cleaning activity compared to Pilkington reference samples. ActivTM. Photocatalytic results showed a TiO_2 film with a thickness of 190 nm from 0.1 M The solution in 7 spray cycles showed the best particle structure and

the best photocatalytic action. Activity that results in 94% stearic acid degradation in 180 minutes under UVA light at reaction rate Constant k = 0.01648rpm[56].

10. Miao Yu et al. (2020): Perovskite solar cells (PSCs) with high power conversion efficiency (PCE) are mainly Mesoporous structures containing mesoporous titanium oxide (TiO_2), a major factor in reducing total content Hysteresis. However, existing manufacturing approaches for mesoporous TiO_2 generally require high temperatures. Annealing process. In addition, there is still a long way to go to improve in terms of increasing electrons. Reduced conductivity and charge carrier recombination. Here is a simple one-step in situ and low temperature procedure Designed to produce compact mesoporous Nb: TiO_2 layers that act as both frameworks and electrons Transport layer (ETL) of PSC. ETL-based compact mesoporous Nb: TiO_2 PSC suppresses hysteresis and This is due to the increased interfacial synergies caused by the morphology of the nanopins. And enhanced carrier transport caused by Nb doping. Such a high quality compact mesoporous layer PSCs assembled using optimized 2% Nb-doped TiO_2 enable an amazing PCE of 19.74%. This paper work Based on compact mesoporous polymers, it promises an effective approach to producing highly efficient PSCs without hysteresis. Structure with low energy consumption and cost[21].

11.Celine Duoont et al. (2020): The surface structure of the Mg dope tiltyl TiO_2 surface in this study was Photoelectron emission and photoelectron diffraction (PED) in the nuclear level / valence band are too evolutionary Algorithms, density functional theory (DFT) and multiple scattering calculations. When the reduced crystal is annealed above 620K, Mg precipitates from TiO_2 by substituting with a Ti atom. A grid that maintains a well-known reconstruction of magnesium-free surfaces. The bandgap state is Completely cured by the separation of Mg, charge compensation is provided by O vacancies, as formally represented by the Kröger and Vink notations. Full support for these results The DFT calculation is based on insights from evolutionary algorithmic calculations that show that the combination of the four surface structures fully explains the observed experimental Ti3s and Mg2s patterns. These model structures contain only Mg at the replacement position There are no interstitial atoms or excess electrons experimentally, but O vacancies Recognized[57].

12.Gaurav K. Upadhyay et al.(2020): After synthesizing various bulk compositions of CdO: TiO_2 and depositing a thin film on a glass substrate by spin coating technology, the composition of CdO: TiO2 was optimized and grown on pSi for solar cell applications. .. The results of XRD show that by increasing the volume fraction of TiO_2 in CdO, Ti^{+4} ion is occupied at the interstitial position or produces Cd. The +2 ion vacancies in the CdO lattice cause a increase in the peak intensity of the CdO cubic structure. The continuous change in surface morphology of from nanoparticles to creeks was studied by FESEM. Using a UV-Vis spectrophotometer, transmission was recorded in the wavelength range of 300- nm to 800 nm, the optical bandgap was reduced by 4344 from 2.38 eV to 1.70 eV, and

the TiO_2 volume ratio of CdO was increased. I found out. The minimum resistance value was obtained as 2 x $10^2\Omega \cdot$ cm for the optimized thin film. A current density-voltage curve (JV) of was used to estimate the curve factor (0.53) and conversion efficiency (3.23%) of the device optimized under with 100 mW / cm2 illumination. .. The overall study is that CdO: TiO_2 nanocomposites By adding TiO_2, we succeeded in reducing the toxicity of CdO and improving the conductivity[23].

13. I Darmadi *et al (*2020) :This publication is a coprecipitation method for synthesizing T-doped ZnO nanoparticles with different Ti contents. Elemental analysis is then performed using energy-dispersed X-ray spectroscopy and the Ti content varies from 5 atomic%, 7 atomic%, and 12 atomic% to 16 atomic% at that atomic percentage of . Revealed. Characterizing the characteristics of the sample structure prepared by X-ray diffraction spectroscopy (XRD), Ti-doped ZnO has an anatase structure in which the lattice constants a = b and c are reduced from 3.251 and 5.213 Å to 3.254 and 5.203 Å. I found that I have it. Ti salary increased It was also found that the particle size of Fe-doped TiO_2 decreased from 12 nm, changing from 5 at% to 16 at%. Up to 10 nm with increasing Ti content, the molecular vibrations of sample by Fourier transform infrared (FTIR) spectroscopy and the optical properties by diffuse reflection UV-Vis spectroscopy were also characterized. The results show that the bandgap energy of Ti-doped ZnO is reduced from 3.20 eV to 3.12 eV, indicating that the photocatalytic activity of Ti-doped ZnO is reduced. After studying the decomposition of methylene blue from aqueous solution under UV irradiation, found that the photocatalytic Ti-doped ZnO had good decomposition at a decomposition rate of about 80%[58].

14.Gourav Mishra et al. (2019): TiO2 @ HNT was prepared by insitu synthesis of TiO_2 nanoparticles. The surface of functionalized halloysite nanotubes (HNT). Photocatalytic PVC film TiO_2 @ HNT M2 (2 wt%) and TiO2 @ HNT M3 (3 wt%) were also prepared. Using the photocatalyst TiO_2 @ HNT and the photocatalytic PVC film, we studied the photocatalytic activity of the dye methylene blue (MB) and rhodamine B (RB) in a UV batch reactor. The structure and morphology of the photocatalyst and photocatalyst PVC film are Fourier transform infrared spectroscopy (FTIR), X-ray diffraction (XRD), scanning electron microscope (SEM), energy dispersed X-ray (EDX), transmission electron. Characterized by microscopy. Electron microscope (TEM). , UVVis spectrophotometer and photoluminescence (PL). PL studies have shown that oxygen vacancies and surface hydroxyl groups present on the surface of TiO_2 @ HNT act as excellent carrier traps and reduce electron-hole recombination rates. TiO2 @ HNTs 2 (2 wt%) and TiO2 @ HNTs 3 (MB dyes degraded at 3 wt% up to 83.21%, 87.47%, RB dyes up to 96.84% and 96, .87% respectively. The TiO_2 @ HNT photocatalyst was found to be stable during three consecutive cycles of photocatalytic decomposition of the RB dye. TiO2 @ HNTs M2 and TiO2 @ HNTs M3 decomposed MB dyes up to 27.19% and 42.37% and RB dyes up to 30.78% and 32.76%. Photocatalytic degradation of both dyes followed the frstorder Kinetic

model. Analysis of the degradation products was performed by liquid chromatography-mass spectrometry (LCMS) and the results showed that dye degradation was initiated by demethylation of molecules. MB and RB dye degradation reactions were tested using TBA and IPA as OH * and H + Scavenger , respectively. The mechanism of photocatalytic activity of TiO_2 @ HNTs and the PVC photocatalytic membrane was also explained[59].

15.Jae Bum Jeon et al. (2019) : The electron selection layer is important for the efficiency, stability and hysteresis of perovskite solar cells. Optical annealing is a low cost roll-to-roll compatible process that can be applied to the post-treatment manufacturing of sol-gel based metal oxide layers. Here, a UV optical annealing system is used to produce an amorphous titanium oxide electron selective film at a low temperature of in a dry atmosphere, which is compared to the thermal annealing process. Reactive oxygen species are produced by UV light to promote hydrolysis and condense TiO_2. A precursor that effectively removes organic ligands. The TiO_2-based photoannealed perovskite solar cell has a power conversion efficiency of 19.37% and no hysteresis[60].

16.Rehab Ramadan et al. (2019): Ti-doped ZnO skinny movies had been acquired with the purpose of tailoring ZnO movie bioadhesiveness and making the optoelectronic houses of ZnO substances transferable to organic environments. The movies had been organized on silicon substrates via way of means of sol−gel spin-coating and next annealing. A Ti−O segregation limits the ZnO crystallite increase and creates a buffer out-layer. Consequently, the Ti-doped ZnO gives barely expanded resistivity, which stays withinside the order of 10−three Ω·cm. The robust biochemical interference of Zn^{2+} ions launched from natural ZnO surfaces become evidenced via way of means of culturing Staphylococcus epidermidis with and with out the Zn^{2+} coupling agent clioquinol. The Ti-doped ZnO surfaces confirmed a sizable boom of bacterial viability with admire to natural ZnO. Cell adhesion become assayed with human mesenchymal stem cells (hMSCs). Although hMSCs locate problems to stick to the natural ZnO floor, they regularly amplify at the floor of ZnO whilst the Ti doping is expanded. A initial microdevice has been constructed at the Si substrate with a ZnO movie doped with 5% Ti. A one-dimensional micropattern with a zigzag shape indicates the choice of hMSCs for adhesion on Ti-doped ZnO with admire to Si. The triggered comparison of floor anxiety in addition induces a mobileular polarization impact on hMSCs. It is suggested that the presence of Ti−O covalent bonding at the doped surfaces offers a miles greater solid floor for bioadhesion. Such fouling conduct shows a power of Ti doping on movie bioadhesiveness and units the start line for the choice of highest quality substances for implantable optoelectronic devices[61].

17.H.P. Shivaraju et al. (2017): Designing photocatalytic materials with modi fied functionalities for the utilization of renewable energy sources as an alternative driving energy has attracted much attention in the area of sustainable wastewater treatment applications. Catalystassisted advanced oxidation

process is an emerging treatment technology for organic pollutants and toxicants in industrial wastewater. Preparation of visiblelightresponsive photocatalyst such as Mgdoped TiO_2 polyscales was carried out under mild sol–gel technique. Mgdoped TiO_2 polyscales were characterized by powder XRD, SEM, FTIR, and optical and photocatalytic activity techniques. The Mgdoped TiO_2 showed a mixed phase of anatase and rutile with an excellent crystallinity, structural elucidations, polyscales morphology, consequent shifting of bandgap energy and adequate photocatalytic activities under visible range of light. Mg-doped TiO_2 polyscale Their effectiveness in degradation was studied The most commonly used industrial dyes in the real-time textile industry sewage. Mg-doped TiO_2 polyscale demonstrated excellent performance Photocatalytic decomposition efficiency in both models Industrial dyes (65-95%) and textile waste liquids (92%) Under natural light as an alternative and renewable Drive energy[17].

18.M.I. Khan et al. (2017): 1, 3, 5, and 7 layers of magnesium-doped titanium dioxide (Mg: TiO_2) thin films are deposited on the FTO glass substrate. XRD shows that changing the number of coating layers changes the phase of TiO_2. The 7th layer film has a larger particle size than the other layered films. According to the absorption spectrum recorded by the UV-Vis spectrometer, as the number of stacked layers increases, the absorption shifts towards the visible region. The gap energies (Eg) of the optical band of the 1, 3, 5, and 7-layer films are 3.48, 3.34, 3.14, and 2.98 eV, respectively. 5 and 7 layer film is 5.68x105 , 1.67x105 , 3.99 x 104 or 6.34 x 102 (Ωcm). 7 The efficiency of the DSSC based on the layer is 1.68%, which is almost 65% better than the DSSC based on the single layer (that is, 1.10%). This improvement in efficiency is due to an increase in particle size and a decrease in Eg[62].

19.Dong Geon Lee et al. (2017): Mesoporous TiO_2 ($mpTiO_2$) layers are commonly used as electron transport layers in perovskite solar cells. Cells that help extract and transport electrons to and from the light-absorbing perovskite layer electrode. Here, we show the results of investigating the effects of the layer thickness of $mpTiO_2$ and the particle size of TiO_2. Regarding photovoltaic characteristics related to the interface with the surface of Mp layer mp layer TiO_2 nanoparticles. Various $mpTiO_2$ layers with thicknesses of 150, 250 and 400 nm Then, we prepared particle sizes of 25 nm and 41 nm and compared their photovoltaic characteristics. Layer with perovskite solar cells. Time-resolved photoluminescence attenuation and impedance studies We have shown that the interfacial resistance and charge injection of perovskite in TiO_2 are important factors. Impact on the performance of photovoltaic power generation. Increased deterioration of photovoltaic parameters We have also confirmed that the TiO_2 / TiO_2 interface region needs to reduce the interfacial series resistance due to these compounds in order to improve the performance of mesoscopic[63].

20.Domian Wojcieszak et al. (2017): Structure and photocatalytic properties of TiO_2 nanopowder doped with 1 at.% cerium, cobalt and copper and iron. Nanoparticles were synthesized by sol-gel

method, SEM, EMF and X-ray method. Furthermore, their photocatalytic activity was determined by the degradation of methyl orange. result Compared to non-alloy powders. Structural studies showed that all prepared nanopowders were nanocrystalline. It had an anatase TiO_2 structure. The average crystallite size is approx. From 4nm to 5nm. The dopant distribution is It is uniform for all powders produced. In addition, in the case of TiO_2 doped with Co, Ce, and Cu, the agglomeration effect was not so great. More than TiO_2:Fe. As a result of the photocatalytic decomposition, all of the obtained nanopowders showed self-cleaning activity. higher than non-alloyed. The efficiency of this reaction (after 5 hours) makes it possible to order nanopowders. as: TiO_2:Co > TiO_2:Ce > TiO_2:Cu > TiO_2:Fe > TiO_2[64].

21.Jo Saito et al. (2017): Organic-inorganic hybrid heterojunction solar cells containing pervoskite $CH_3NH_3PBI_3$ using Nb, Ta, pr v-doped TiO_2 were fabricated and characterised . By doping Nb , the conductivity and carrier density of the TiO_2 increased , and its flat-band potential showed a positive shift. The short-circuit current density and power conversion efficiency of pervoskite solar cells were improved by using $T_{io.95}\,Nb_{0.05}O_2$ compared to undoped TiO_2[65].

22.M.Asemi et al.(2016): Introduce MgO insulating layer at TiO_2 electrolyte interface to improve power conversion efficiency of DSSC Suppress and reduce charge recombination rate Electron transfer from TiO_2 to the electrolyte. The thickness of the MgO layer is Dye-sensitized solar cells affect overall efficiency Cell with optimized efficiency MgO layer thickness Highest conversion efficiency (g = 5.12%) High short-circuit current density (18.15 mA / cm^2) Open circuit voltage (0.571V). Open circuit voltage The attenuation measurement result is Surface modification due to charge delay Electronic lifetime of DSSC manufactured with optical anode Recombinant. Explore the reason for JSC Improved, incident photon current conversion efficiency Conducted efficiency measurement. Our result is Improves the life of light-injected electrons Contributes to improving electronic collection efficiency Increases efficiency and improves JSC score. In addition to it Enhanced photoinjected electron recombination Velocity is also indicated by electrochemical impedance[66].

23.Ardeshir Baktash et al. (2016): The effects of magnesium-doped TiO_2 and ZnO as whole-blocking layer (HBL) are studied using the Solar Cell Capacitance Simulator (SCAPS). We will study the effect of the concentration of magnesium in TiO_2 and ZnO and the effect of operating temperature on the performance of the perovskite solar cell . The highest cell performance in both TiO_2 and ZnOHBL (with cell efficiencies of 19.86% and 19.57%, respectively) can be concluded when the structure of HBL is doped with 10% Mg into . The performance of perovskite solar cells, which raise the operating temperature from 300K to 400K, deteriorates in both pure HBL and Mg-doped HBL. However, cells with pure ZnO layers and Zn0.9 Mg0.1O layers show the highest (8.88% efficiency at drops) and lowest stability (50.49% efficiency at drops) at high temperatures. Or even more, cells with a Ti0.9

$Mg0.1O_2$ layer have better stability (efficiency 21.85) than cells with a pure TiO_2 compact layer (efficiency reduced by 21.4423.28%) at higher operating temperature[67].

24.Ali A. Yousif et al. (2016): Silver-Ag-doped titanium dioxide nanocrystal TiO_2 membrane deposited at $(TiO_2)_{1x}(Ag)_x$ at concentrations different from x = (0, 0.01, 0.02, 0.03, 0.04 and 0, 05) Wt. The was manufactured on a glass substrate by pulsed laser deposition (PLD) using a pulsed NdYAG laser with wavelength (λ = 1064 nm), duration (9 ns) and energy (700 mJ). This study included a study of optical properties by measuring absorption and transmission spectra in the wavelength range (3201100) nm. The results show that the film has a high transmittance for all films, is about 6094% in spectral visibility and NIR, and can be used as an optical window for solar cells. The results show that the absorption coefficient has a controlled direct transition. The energy gap value is calculated from the direct electronic transitions allowed in and is (3.813.63) eV. The energy gap gradually decreases as the impurity ratio decreases[22].

25.Chenxi Zhang et al.(2016): Light-absorbing organolead trihalide perovskite materials have been successfully employed in efficient photovoltaic (PV) cells. Cell architectures based on mesoscopic metal oxides and planar heterojunctions have already made significant and rapid progress, with a lot of room for improvement PV technology that is well-established. The high power conversion efficiency (PCE) values came from a few hundred nanometer thick mesoporous scaffold (e.g. TiO_2 or SiO_2) is used in a mesoscopic configuration.Perovskite absorber-infiltrated Al2O3 was placed between the electron and hole transport layers.For high efficiency perovskite-based thin films, a homogenous and compact hole-blocking layer is required solar panels Various approaches were used to investigate the features of TiO_2 compact layer in this study and its impact on perovskite solar cells' PV performance.A sol-gel approach based on titanium isopropoxide and HCl, spin-coating of titanium diisopropoxide bis (acetylacetonate), screen-printing of Dyesol's bocking layer titania paste, and a chemical bath deposition (CBD) technique based on hydrolysis of $TiCl_4$ were used to create TiO_2 compact layers. Scanning electronic microscopy and X-ray diffraction were used to examine the morphological and microstructural properties of the compact TiO_2 layers that had been created. The surface morphologies of TiO_2 compact films played a crucial role in impacting the efficiencies, according to the analysis of device performance parameters. The CBD-deposited nanocrystalline TiO_2 film is the most effective hole-blocking layer and produces the best performance in perovskite solar cells.The CBD-based TiO_2 compact and dense layer inside the device has a low series resistance and a strong recombination resistance, allowing for a high power conversion efficiency of 12.80 percent[68].

26.Mantas Sriubas et al. (2015): Energy-dispersive X-ray spectroscopy, X-ray diffraction (XRD), and an impedance spectrometer were used to evaluate Mg-doped TiO_2 thin ceramic films produced by e-beam deposition. The effect of Mg dopant concentration and a careful analysis of the kinetics of

electrical charge carrier transport in thin films.The structural characteristics and nonlinear behaviour of electrical conductivity were altered by concentration of the very thin films With the drop in temperature, XRD examination indicated anatase structure in TiO_2 thin films crystallinity by increasing the Mg dopant concentration Conductivity total and activation Mg content and ambient temperature affect energy. Total conductivities with the greatest values 1.2 mol percent (873 K) and 2.5 mol percent (873 K) were used to achieve 6.17E-6 and 5.50E-4 S/cm, respectively (1230 K) corresponding dopant concentrations[29].

27.Nannan zhao et al. (2014): Optimizing the source/drain materials improves the performance of Titanium-doped Zinc-oxide (TZO) Thin-Film-Transistors (TFTs). We have successfully manufactured TZO TFTs using a variety of source/drain materials, including AI, Mo, Cr, Mo/AIIMo, and Cr/AIICr. During each deposition phase, there is no deliberate substrate heating, and the highest process temperature is 80°C. TFTs with Cr/ AIICr as source/drain have excellent electrical properties, with a high saturation mobility of 171.4 cm2y.1 S1, a low sub threshold swing (SS) of 0.25 Y/decade, a high off ratio of 2xl08, and a threshold voltage (Y^{th}) of 3.0Y[69].

28.Tong Sun et al. (2014): To investigate the relationship between the microstructures of titanium-doped ZnO powders and their antibacterial characteristics, alcohothermal titanium-doped ZnO powders of various forms and sizes were produced from various zinc salts. The antibacterial activities of titanium-doped ZnO powders on Escherichia coli and Staphylococcus aureus were evaluated using X-ray powder diffraction (XRD), Fourier transform infrared spectroscopy (FT-IR), ultraviolet-visible spectroscopy (UV-vis), scanning electron microscopy (SEM), transmission electron microscopy (TEM), and selected area electron diffraction (SAED). SEM was used to characterise the tested strains, as well as the electrical conductance variation trend of the bacterial sample. The results show that the powders have distinct morphologies due to the different zinc salts used in their production.The XRD results show that samples made from zinc acetate, zinc nitrate, and zinc chloride are zincite ZnO, whereas samples made from zinc sulphate are a mixture of ZnO, $ZnTiO_3$, and $ZnSO_4$ 3Zn $(OH)_2$ crystal. The absorption margins of titanium-doped ZnO powders made from zinc acetate, zinc nitrate, and zinc chloride are red shifted to more than 400 nm, according to UV-vis spectra. Titanium-doped ZnO powders produced from zinc chloride have excellent antibacterial action, with minimum inhibitory concentrations (MIC) and minimum bactericidal concentrations (MBC) of less than 0.25 g L1. Similarly, when bacteria are treated with ZnO powders made from zinc chloride, the bacterial cells are severely injured, and bacterial electrical conductivity increases[20].

29.Mantas Sriubas et al.(2014): Due to its unique dielectric, electrochemical, photocatalytic, and optical properties, titanium dioxide is regarded as one of the most important compounds. By injecting a specific number of dopants, these qualities can be changed. The structural and electrical characteristics

of Ca-doped titanium dioxide were examined using the electron beam deposition method. X-ray diffraction (XRD), energy dispersive spectroscopy (EDS), and scanning electron microscopy were used to evaluate the structural properties of the produced thin ceramic films (SEM). Impedance spectroscopy was used to analyse electrical properties. It was discovered that when the concentration of Ca dopants grows, so does the size of the crystallites, following Vegard's law. Ca-doping reduced the overall conductivity of the produced thin films, according to impedance measurements.Under wet reducing circumstances, the total conductivity ranges from 2.7 S/cm in pure TiO_2 to 4 10^{-4} S/cm in 2.5 percent Ca doped TiO_2 at 800 °C, and from 5.4 10^{-4} S/cm in pure TiO_2 to 3.4 10-5 S/cm in 0.5 percent Ca doped TiO_2 at 800 °C[19].

30.Qiuping Liu (2014): The hydrothermal approach was used to create Mg salts [$Mg(NO_3)_26H_2O$]-doped TiO_2 electrodes that were well optimised. The TiO_2 or Mg-doped TiO_2 slurry was deposited onto the fluorine-doped tin oxide glass substrate by the doctor blade method and sintered at 450°C to make the working electrode. The doped Mg ions exist in the form of Mg^{2+}, which can act as e or h^+ traps and reduce the e/h^+ pair recombination rate, according to X-ray photoelectron spectroscopy (XPS) data. The Mg-doped TiO_2 photoanode shifts the flat band potential favourably, according to the Mott-Schottky plot. The increased driving power of injected electrons from the dye's LUMO to the TiO_2 conduction band is due to the positive shift of the flat band potential. The photovoltaic efficiency in this investigation was 7.12%. This study shows a photovoltaic efficiency of 7.12%, which is higher than the undoped TiO_2 thin film's (5.62%), and a 26.7 percent increase in short-current from 14.9 to 19.1 mA[70].

31.T.Siva Roa et al. (2012): The photocatalytic activity of TiO_2 was investigated using magnesium doping (Mg^{2+}-TiO_2) with magnesium weight percentages ranging from 0.75 to 1.5 wt%. X-ray diffraction (XRD), N_2 adsorption-desorption (BET), X-ray photoelectron spectroscopy (XPS), UV-visible diffuse reflectance spectroscopy (DRS), and scanning electron microscopy were used to examine the doped and undoped materials (SEM). The anatase crystalline phase was seen with Mg2+-TiO2 catalysts, showing that Mg^{2+} ions had no effect on TiO_2 crystal patterns. XPS spectra were used to determine the presence of magnesium ions in the TiO_2 matrix. For doped TiO_2, DRS spectra revealed a considerable absorption shift towards the visible range. Doped catalyst has smaller particle size and higher surface area than undoped TiO_2, according to SEM pictures and BET measurements. The photocatalytic degradation of aqueous dichlorvos (DDVP) under visible light irradiation was used to test the photocatalytic efficiency of the produced catalysts, and it was discovered that Mg^{2+}-doped catalysts have greater catalytic activity than undoped TiO_2. This is due to the fact that Mg^{2+}- TiO_2 creates electron-holes more efficiently in visible light than undoped TiO_2, which can only be stimulated

by UV irradiation. The effects of dopant concentration, solution pH, catalyst dosage, and beginning pesticide concentration have all been investigated[16].

32.Mohammad A. Behnajady et al. (2011): Sol-gel technique was used to make TiO_2- and Mg-doped TiO_2 nanoparticles with dopant concentrations. X-ray diffraction (XRD), scanning electron microscopy (SEM), transmission electron microscopy (TEM), Brunauer–Emmett–Teller (BET), and diffuse reflectance spectroscopy (DRS) techniques were used to analyse the produced photocatalysts. The BET analysis revealed an 8 nm pore diameter and a surface area of 48.5 m^2 g)1. At 450 degrees Celsius, XRD patterns of pure and doped TiO_2 nanoparticles revealed that all phases are anatase. TEM revealed a particle size of less than 20 nm. Mg-doped TiO_2 nanoparticles had a smaller band gap energy than TiO_2 nanoparticles. The photocatalytic activity of pure and doped nanoparticles in the elimination of C.I. Acid Red 27 was compared (AR27).For the breakdown of AR27, Mg-doped (0.2 mol percent) TiO_2 had a greater photocatalytic activity than bare TiO_2 nanoparticles. Total organic carbon analysis and alterations in the AR27 UV–Vis peaks revealed that Mg-doped TiO2 nanoparticles may achieve 99 percent mineralization and extinguish all UV and visible peaks. AR27's removal effectiveness was affected by factors such catalyst dose, pollutant concentration, and light intensity.The initial pesticide concentration and catalyst dosage have been investigated[71].

33.J. Olea et al. (2008): Ti ion implantation at large dosages into Si has been accomplished. The maximal average of substitutional Ti atoms after laser annealing is around 1018 cm^3. At room temperature, Hall effect studies reveal n-type samples with mobility values of around 400 cm^2 /V s. These findings show that the solid solubility limit of titanium in Si has been greatly exceeded without the creation of a titanium silicide layer. This was a promising breakthrough in the pursuit of an intermediate band in Si, allowing the development of a new generation of high-efficiency solar cells based on Ti implanted Si wafers[73].

2.3. CONCLUSION:

Various works on various materials have been identified by a review of the literature. Literature evaluations on thin films made using Mg doped TiO_2 materials employing various preparation procedures were provided. We can learn about the qualities of various materials through these reviews. These past work's results will be useful in analysing our work's outcome. These publications will be useful in comparing our results. The brief examination of literatures provided above will be valuable in learning about the materials and in carrying out our project work.

CHAPTER-3

MATERIALS AND METHODOLOGY

3.1. INTRODUCTION:

This chapter deals with the details about the materials used. Different Experimental techniques were explained in this chapter. Different deposition techniques are explained among which Spray pyrolysis using nebulizer is used for coating the glass substrate. Thin films were prepared. The preparation and characterization were explained in this chapter.

3.2.THIN FILM DEPOSITIONS:

Thin film deposition technologies are classified as either fully physical (evaporative methods) or purely chemical (gas and liquid phase chemical processes). A large number of techniques based on glow discharges and reactive sputtering combine physical and chemical reactions, and are thus classified as physical-chemical approaches. Thermal evaporation, also known as vacuum evaporation, is one of the oldest processes for forming thin films and is still frequently employed in the laboratory and industry for depositing metals and metal alloys. Thin film solar cells have been developed to lower production costs.

There are two types of thin film deposition techniques:

i)physical deposition and

ii)chemical deposition.

3.3.PHYSICAL VAPOR DEPOSITION:

Thermal evaporation, electron beam evaporation, sputtering, closed space vapour transport [CSVT], atomic layer deposition [AID], brush plating, hot wall deposition [HWD], and pulsed laser deposition are examples of physical deposition techniques.MBE [molecular beam epitaxy] with laser deposition.

3.3.1. EVAPORATION TECHNIQUES:

The widespread deposition of materials in the form of thin-layer films is referred to as evaporation processes. The general mechanism of these approaches is achieved by changing the phase of the substance from solid to vapour and then back to solid on the chosen substrate. It takes place in a vacuum or in a controlled environment.

3.3.1.1. VACCUM THERMAL EVAPORATION TECHNIQUE:

The easiest way for making amorphous thin films, especially chalcogenide films like CdSSe, MnS, Ge-Te-Ga, and so on, is vacuum evaporation. Chalcogenide materials can be employed for memory switching, phase-change materials, and solar applications in general.Thermal evaporation relies heavily on two factors: thermally evaporated material and imparting a potential difference to the substrate at a vacuum level of 10^{-5} to 10^{-9} mbar. The diagram for thermal evaporation was copied from somewhere else.

3.3.1.2. ELECTRON BEAM EVAPORATION:

Another form of physical deposition is evaporation, in which an intense beam of electrons is created from a filament and guided through both electric and magnetic fields to hit the target and vaporise it in a vacuum environment. Electron beam evaporation thin films are of high quality and purity.The electron beam evaporation process can be used to make a variety of materials, including amorphous and crystalline semiconductors, metals, oxides, and molecular compounds.

3.3.1.3.LASER BEAM EVEPORATION:

Another physical deposition technology for the thin film coating system is pulsed-laser deposition (PLD). The laser beam is used to ablate the material for depositing thin films inside a vacuum chamber during the thin film deposition process.To ablate the target, various types of laser sources are used. Nd-YAG lasers, KrF (248 nm), and XeCl are the most popular sources (308 nm). When a laser beam hits a target substance, it creates a plume that can deposit on a variety of substrates. Ionized species, as well as neuronal and ground-state atoms, may be found in the plume. The oxides of metals are deposited using oxygen in metal oxide thin films. The thickness of the thin layer produced by the PLD is determined by a number of factors, including the laser's wavelength, energy, ambient gas pressure, pulsed duration, and the target's distance from the substrate.Laser-induced fluorescence, laser ablation molecular isotopic spectroscopy, and optical emission spectroscopy can all be used to regulate and monitor the ablation process during deposition. The substrate temperature has an impact on the shape of the deposited thin films. PLD is used to coat thin films in three ways: Frank—van der Merwe, Stranski—Krastanov, and Volmer—Weber. Because of its quick deposition time and compatibility with oxygen and other inert gases, PLD has some benefits over other physical deposition techniques.

3.3.2.SPUTTERING TECHNIQUES:

Sputtering is a process for forming metal and oxide coatings in which the crystalline structure and surface roughness are controlled. The simplest sputtering system consists of an evacuated chamber housing a metallic anode and cathode for obtaining a glow discharge in the chamber's residual gas. In addition, film deposition can be achieved with a voltage of several keV and a pressure of more than

0.01 mbar.The sputtering process is based on the bombardment of the molecules in the cathode with ions produced by the discharge, resulting in higher kinetic energy liberation of the molecules from the cathode. To maximise momentum transfer, the bombardment ions' atomic weight should be close to that of the target material. These molecules travel in straight lines and collide with the anode or substrate, forming a dense thin coating.

3.3.3.CHEMIVAL VAPOR DEPOSITION:

Although physical methods for producing thin films provide superior quality and functionalize qualities, they are expensive and may necessitate a huge amount of material target Advance Deposition Techniques for Thin Film and Coating. Chemical deposition techniques are widely employed around the world due to the necessity to manufacture high-quality thin films at a reasonable cost. These methods are inexpensive and produce high-quality films. The majority of them do not necessitate the purchase of pricey equipment. Chemical deposition is highly influenced by the chemistry of solutions, pH, viscosity, and other factors. Solgel deposition, chemical bath deposition, electrodeposition, chemical vapour deposition (CVD), and spray pyrolysis are the most prevalent chemical deposition techniques.

3.3.3.1.SOL-GEL TECHNIQUE:

For the manufacture of oxide compounds, the sol-gel method is widely utilised . One of the most well-known wet-chemical processes is the sol-gel procedure. It works with lower-temperature processing and improves multicomponent material homogeneity. The term "sol" refers to the production of a colloidal suspension, whereas "gel" refers to the transformation of a colloidal suspension into viscous gels or solid solids. The following are two methods for making transition metal oxides (TMOs):

a. Preparation of inorganic precursors in aqueous solution using inorganic salts

b. Preparation of metal alkoxide precursors in nonaqueous solvents using metal alkoxides.

3.3.3.2. DIP COATING:

Dip-coating is nearly always utilised to create transparent oxide layers on a transparent substrate with excellent planarity and surface quality. Other substrates can be used as well. Film thicknesses of up to 1 m can be deposited with precision. Several additive layers can be layered on top of each other.Immersion, start-up, deposition, drainage, and evaporation are the five steps of the dip-coating process, according to Scriven. As a result, evaporation is usually associated with the start-up, deposition, and draining processes.

3.3.3.3. SPIN COATING TECHNIQUE:

After the precursor solution is prepared, another technique known as spin coating or spinning is available for use. The solution is dropped uniformly onto a spinning substrate. The spinning procedure is best for coating small discs or lenses, although it is not particularly cost-effective.

3.3.3.4. CHEMICAL BATH DEPOSITION:

Solution growth technique or controlled precipitations are other names for the chemical bath deposition method. It is the most ancient method of film deposition on a substrate. The solution growth technique is commonly used to make chalcogenide and metal oxide films. The deposition can also be carried out at lower temperatures. The precursor solution of metal ions must be complexed by ligands in the solution growth process. Ammonia solution, triethanol amine, ethylene-diamine-tetraacetic acid (EDTA), citric acid, and other compounds are almost all used to make the complex solution. After the complexation has been finished, the anions should be added. The sulphur anions come from thiourea, thioacetamide, thiosulfate, and sodium Sulfide solutions, whereas the selenium anions come from selenourea and sodium selenosalfate.Inside the solution, substrates are placed in a vertical, horizontal, or particular position and left until the desired film thickness is achieved. The deposition of oxide coatings differs significantly from that of chalcogenides. After completing the complexation by adjusting the pH value, the substrate is immersed in the solution at a temperature ranging from 60° to 100°C to deposit metal hydroxide films in the majority of cases.The annealing procedure can then convert the hydroxide coating to oxide[26].

3.3.3.5. SPRAY PYROLYSIS:

The decomposition of chemical substances or solutions under the influence of heat at extremely high temperatures is referred to as paralysis. The word paralysis is derived from the Greek words pyro (heat) and lysis (lysis) (breaking). Pyrolysis is defined as a transformation caused by heat. Part of a complex is broken.The process of breaking down a molecule into simple units with heat is known as paralysis. It has a number of advantages, including a low cost.Temperature of processing, product uniformity and purity, and so forth. The chemical spray causes a coma technology (SPT) has been one of the most essential techniques in the previous three decades a broad variety of materials can be deposited in a thin layer It has a number of advantages, including minimal processing time[27].

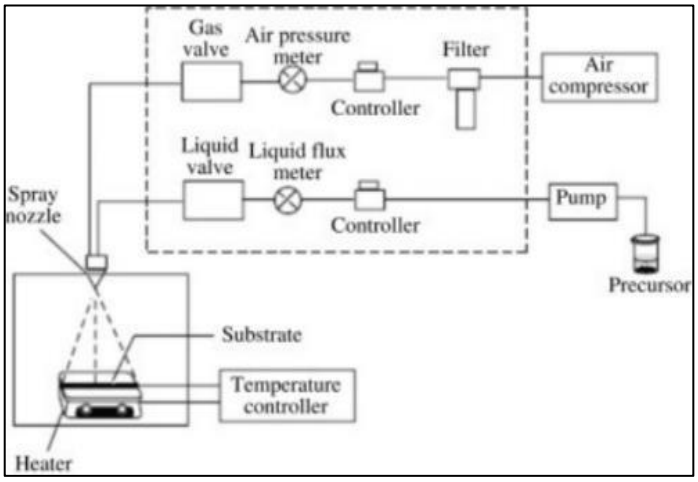

Fig.3.1:Spray Pyrolysis process

3.4.SOURCE MATERIALS:

- ***MAGNESIUM ACETATE TETRAHYDRATE:***

Magnesium acetate tetrahydrate is a form of hydrated acetate of magnesium. Magnesium is a divalent cation essential for many biochemical processes involved in neural signaling, bone calcification, and muscle contraction. About 350 enzymes involved in glycolysis and the Krebs cycle, cyclic AMP and ATP formation, cell signaling, and protein and nucleic acid synthesis are dependent on magnesium.

Magnesium acetate tetrahydrate is a hydrate of anhydrous magnesium acetate salt with the chemical formula Mg (CH3COO) 2 • 4H2O. As a form of magnesium salt, magnesium acetate is one of the most biologically available forms of magnesium, forming highly water-soluble compounds. Magnesium is an essential element and is the second most abundant cation in the body to play an important role in maintaining normal cellular functions such as ATP production and efficient enzyme activity. Magnesium acetate tetrahydrate can be used as an electrolyte supplement or as a reagent for molecular biology experiments[32].

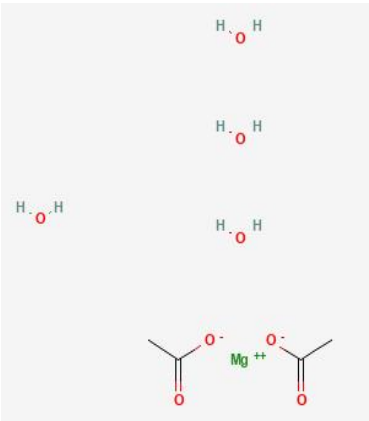

Fig.3.2:Magnesium Acetate Structure

❖ ***TITANIUM ISOPROPOXIDE:***

The chemical formula for this alkoxide is $C_{12}H_{28}O_4Ti$.

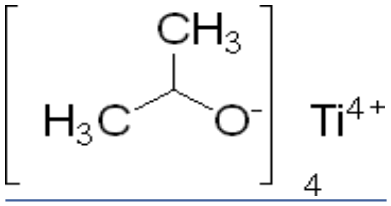

Fig.3.3:Titanium Isopropoxide

Ti is a chemical element with the atomic number 22 and the atomic weight 47.90. As a member of the first transition group, its chemical behaviour is very similar to that of silica and zirconium. Its chemistry in aqueous solution, particularly in lower oxidation states, is similar to that of chrome and vanadium. Titanium is a light transition metal with a white-silvery metallic appearance. It's tough, lustrous, and corrosion-resistant. Titanium is insoluble in water but soluble in concentrated acids. When exposed to elevated temperatures in air, this metal forms a passive but protective oxide coating (leading to corrosion resistance), but it resists tarnishing at room temperature.The most common oxidation state is 4+, though 3+ and 2+ are also possible but less stable. When heated to obtain the dioxide, TiO_2, and when combined with halogens, this element burns in the air. It reduces water vapour to form hydrogen and dioxide, and it reacts similarly with hot concentrated acids, though chlorohydric acid forms trichloride. TiH_2 is formed when the metal absorbs hydrogen and forms the nitride (TiN) and carbide (TiC). The sulphur TiS_2, as well as the lowest oxides Ti_2O_3 and TiO, as well as the sulfurs Ti_2S_3 and TiS, are all known compounds. The three oxidation states of salts are known.Titanium is as strong as steel but 45 percent lighter.The dielectric constants of solid solutions of $SrTiO_3$ in $BaTiO_3$ range from 13 for $MgTiO_3$ to billions for solid solutions of $SrTiO_3$. The dielectric constant of barium titanate is 10.000 at 120 ℃ , which is its Curie point, and it has low dielectric hysteresis. In terms of thermal stability, ceramic transducers containing barium titanate outperform Rochelle salt and quartz in terms of effect strength and ability to form ceramics in a variety of shapes. The compound has been used as a sound detector as well as a source of ultrasonic vibrations.The titanium dioxide, TiO_2, is commonly found in the form of rutile, which is black or brownish. The anatasite and brooquite are two natural forms that are less common in nature. Both pure rutile and pure anatasite are white minerals. The black basic oxide, $FeTiO_3$, can be found in nature as the mineral ilmenite, which is the primary commercial source of titanium[14].

❖ ***ISOPROPANOL:***

Isopropyl alcohol (IUPAC name Propan-2-ol, also known as isopropanol or 2-propanol) is a colorless, flammable compound (chemical formula $CH_3CHOHCH_3$) with a strong odor. As an isopropyl group attached to a hydroxyl group, this is the simplest example of a secondary alcohol in which the

carbon atom of the alcohol is attached to the other two carbon atoms. It is a structural isomer of 1-propanol and ether. Used in the manufacture of a wide variety of industrial and household chemicals, it is a common ingredient in chemicals such as preservatives, disinfectants and detergents. In 1920, Standard Oil first produced isopropyl alcohol by hydrating propene. Isopropyl alcohol dissolves non-polar compounds with a wide spectrum of . It also evaporates rapidly, leaves little trace of oil compared to ethanol, and is relatively non-toxic compared to alternative solvents. Therefore, is widely used as a solvent and cleaning solution, especially for dissolving oils.

Fig.3.4:Isopropanol

3.5.PRECURSOR PREPARATION:

The precursor solution is prepared by using the magnesium acetate tetrahydrate, titanium and the isopropanol. The appropriate amount of Magnesium Acetate is measured and taken. The weighed balance is added to the solution of 50 ml solution in a beaker. It is then kept in the magnetic stirrer for an hour to dissolve the salt.

3.6. GLASS SUBSTRATES:

This is the base material on which the deposit takes place. There are two types of boards. They are flexible thin film boards and rigid thin film boards. The thin film substrate changes based on the field. The thin film board used for solar cells is a rigid thin film board. The glass substrate taken is approximately equal in length and width , each about 2.5 cm.

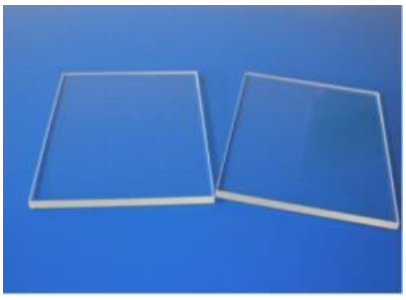

Fig.3.5:Glass plates

3.6.1. CLEANING OF GLASS PLATES:

Cleaning the glass substrate is very important before pre-depositing the glass substrate. This is because impurities in the glass plate affect the separation during the separation. Therefore, first clean the glass substrate to remove foreign matter such as dirt and dust on the glass plate. A clean and tidy glass substrate is needed to achieve the desired result after deposition. There are many cleaning processes in which ultrasonic cleaning is used in this task. First, clean the glass substrate with soap solution. Then, the washed glass substrate is washed again with distilled water of a. Next, place these pieces of glass in an ultrasonic cleaner and hold them at room temperature of about 30 ° C for about 30 minutes. Hold in an ultrasonic cleaner containing soap solution for 30 minutes , then hold in an ultrasonic cleaner containing distilled water at 30 ° C for 30 minutes. Then it is treated with acetone and cotton. Handle with care after cleaning the glass substrate. Must be handled with tweezers and gloves must be worn when handling.

STEPS FOR CLEANING THE GLASS PLATES:

- At first,the glass plates are first cleaned with soap water solution with a cotton.
- They are then cleaned with the distilled water and are cleaned with acetone.
- The glass plates are again cleaned with the soap solution in the ultrasonic bath for 10 minutes.
- Then are cleaned with distilled water for 10 minutes in ultrasonic water bath and are again replaced by acetone for 10 minutes.
- Then the glass plates are taken out from the acetone solution and kept for drying in hot air oven at a temperature of 80℃.

Fig.3.6:Ultrasonic Cleaner

3.7. METHODOLOGY:

- Mg doped TiO_2 was deposited on the TCO coated glass plates by the nebulizer spray pyrolysis technique.
- Magnesium was taken in the molar ratio of 0.1 and added to the Iso-propanol of 50ml.

- Then the solution is kept for stirring in the magnetic stirrer at 70℃ until the salt is dissolved, covered by a butter sheet.
- Then the Titanium Isopropoxide of 6 ml is added to the solution.

Fig.3.7: Precursor solution

- The glass plates are weighted before placing on the hot plate.
- The solution is then coated on the TCO plates which are placed on the hot plates and heated at a temperature of 400℃.
- The distance between the hotplate and the glass tube was about 5 cm .
- The solution is poured into the nebulizer and the solution is coated on the glass plates using the air com-presser with required precautionary steps.

Fig.3.8:During spray

Fig.3.9:Air compressor

- The coated plates are kept for annealing in the muffle furnace for 45 minutes at a temperature of 350℃.
- The glass plates that are coated are again weighted for the calculation.
- The characterization of the plates are taken.

Fig.3.10: Muffle Furnace

3.8.CHARACTERIZATION TECHNIQUES:

3.8.1.X-RAY DIFFRACTION:

X-ray diffraction is currently a common technique for research Of crystal structure and interatomic distance. X-ray diffraction Based on constructive interference of monochromatic X-rays And crystal samples. These x-rays Cathode ray tube filtered to produce monochromatic radiation, collimated to concentrate it, and directed to the sample.If the condition meets Bragg's law, the interaction between the incident ray and the sample causes constructive interference (and diffracted rays).

$$n\lambda=2d\sin\theta$$

Where n is an integer, λ is the wavelength of the X-ray, and d is Is the grid spacing that produces diffraction and θ is Diffraction angle.By scanning the sample in a range of 2θ angles The grid must be achieved due to the random orientation of Powder material. Diffraction peak conversion You can use dispacings to identify the connection. Each connection has its own set of distances. Normal This is achieved by comparing the distance to the standard Reference pattern. The X-ray diffractometer consists of the following three basic elements. X-ray tube, sample holder, X-ray detector[28].

X-rays are generated in the cathode ray tube by heating the filament to generate electrons and accelerating the electrons. Target by applying voltage and shooting the target Material containing electrons. When there are enough electrons Energy that emits electrons from the inner shell of the target material, Characteristic X-ray spectrum is generated. Kα consists of a part Kα1 and Kα2. Kα1 has a bit shorter wavelength and twice the intensity of Kα2. The specific wavelengths are characteristic of the target material (Cu, Fe, Mo, Cr). Filter, by sheet or crystal monometer, is required to produce the monochromatic X-rays required for diffraction. Kα1 and Kα2 are close enough in wavelength so a weighted average of both is used. Dong is most common target materials for single-crystal diffraction.

These X-rays are collimated and directed at the sample. As sample and The detector is rotated, the intensity of the reflected X-ray is enter. When the geometry of the incident X-ray strikes the sample satisfying Bragg's law, the structural interference occurs and an intensity peak occurs[28].

Fig.3.11: X-Ray Diffractometer

A detector records and processes this X-ray signal and converts the signal to a count rate, which is then output to a device such as a printer or computer monitor. The geometry of an X-ray diffractometer is such that the sample rotates in the path of the collimated X ray beam at an angle u while the X-ray detector is mounted on an arm to collect the diffracted X-rays and rotates at an angle of 2u. The instrument used to maintain the angle and rotate the sample is termed a goniometer. For typical powder patterns, data are collected at 2u from 5 to 70 , angles that are preset in the X-ray scan. X-ray powder diffraction is most widely used for the identification of unknown crystalline materials (e.g., minerals, inorganic compounds). Identify the unknown Solids are essential for studies in geology, environmental science, materials science, engineering, and biology. Other Applications include characterization of crystalline materials, determination of fine-grained minerals such as clay and layered clay that is difficult to identify optically, determine the size of the unit cell and measure the purity of the sample. With a specialized technique, X-ray diffraction (XRD) can be used to determine the crystal structure using Rietveld purification, determining the amount of a mineral by the method (quantitative analysis), which characterizes samples with thin layers and make structural measurements, such as the orientation of grains, in a polycrystalline sample[28].

Restriction :

- ✧ Homogeneous material, single phase is best for identification cation of an unknown.
- ✧ Access to a standardized reference file of inorganic compounds needed.
- ✧ Material, in tenths of a gram, to be ground into powder.

- ✧ For composite materials, the detection limit is »2% of sample.
- ✧ For unit cell determination, model indexing for non-isotropic crystalline systems is complicated "reflex"[28].

3.8.2. FTIR SPECTROSCOPY:

Fourier transform infrared (FTIR) spectroscopy is a widely used technique for identify functional groups in materials (gas, liquid and solid) using infrared radiation beam. Infrared spectroscopy measures the absorption of IR radiation emitted by each bond in the molecule and thus produces a spectrum commonly referred to as transmittance % over wave number (cm^{-1})[29].

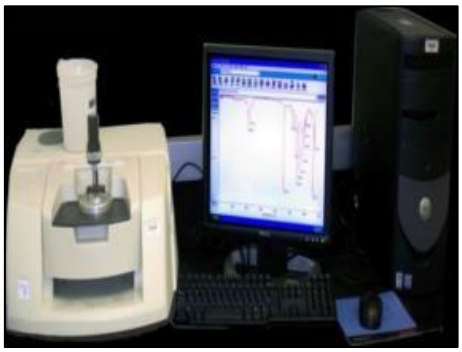

Fig.3.12.FTIR spectroscopy

When infrared radiation is bombarded into the sample, it will absorb light and produce different vibration modes. This absorption is precisely related to the nature of the bonds in molecule. The frequency bands are measured as normal wave numbers on ranges from 4000 to 600 cm − 1. The FTIR spectrum is measured in wave number because wave number is directly related to energy and frequency, providing a simple way to interpret the spectrum. Before sample analysis, the background recorded, to avoid air and water vapor pollution peaks. Ratio of the background noise and the spectrum of the sample is directly related to the absorption sample spectrum. Absorption spectrum shows different oscillations of bonds present in the sample molecule. Some modes arise due to the vibration link. So in this way one can easily define the functional group in a molecule[29].

The ordinary FTIR spectrometer includes an IR mild supply, interferometer, pattern compartment, detector, amplifier, and computer. The mild supply generates radiation which moves the pattern passing via the interferrometer and reaches the detector. Then the sign is amplified and transformed to virtual sign (interferrogram) via way of means of the amplifier and analog-to-virtual converter, respectively. Eventually, the interferrogram is translated to spectrum via the quick Fourier remodel algorithm. Michelson interferrometer is the principle middle of FTIR spectrometer . The interferrometer includes a beam splitter, constant reflect, and a portable reflect that interprets returned

and forth, very precisely. The beam splitter is made from a unique cloth that transmits 1/2 of of the radiation putting it and reflects the relaxation 1/2 of of the radiation. It works on the premise of precept that the mild from the supply is gathered via way of means of collimating reflect and made its rays parallel, which moves beam splitter and therefore splits into beams. One beam is transmitted via the beam splitter to the constant reflect, and the second one is meditated off the beam splitter to the transferring reflect. The constant and transferring mirrors mirror the radiation returned to the beam splitter. Accordingly, each of those meditated radiations are recombined on the beam splitter, ensuing in a single beam that leaves the interferometer and interacts with the pattern and moves the detector. Principally, FTIR (Fourier remodel infrared) is a technique of acquiring infrared spectra, which incorporates first of all the gathering of an interferogram of a pattern sign the use of an interferometer after which overall performance of a Fourier remodel (FT) at the interferogram to acquire the spectrum. An FTIR spectrometer collects and digitizes the interferogram, plays the FT function, and presentations the spectrum.[29].

3.8.3. UV-VIS SPECTROCOPY:

UV-VIS spectroscopy is one of the oldest instrumental techniques for analysis and is the basis for some ideal methods for determining micro and semi-microscopic amount of the analyse in a sample. This is the measurement of consequences of the interaction of electromagnetic radiation in UV and/or the visible areas with absorbent species such as atoms, molecules or ions[30].

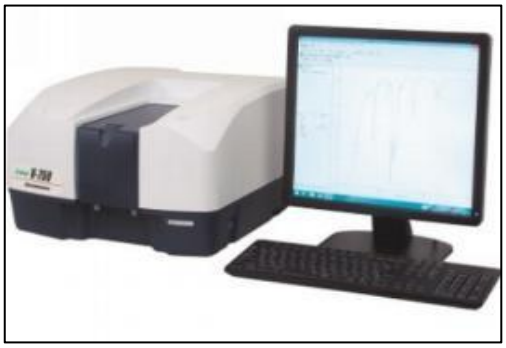

Fig.3.13: UV-VIS Spectroscopy

Ultraviolet and visible light absorption (UV-Vis) spectroscopy is the measurement of attenuation of the light beam after passing through the sample or after reflection a sample surface.The visible spectrum extends from 400 nm to about 800 nm. The color we see depends on wavelength. The color of a substance is determined by the color of its light absorbs and the color(s) it transmits or reflects additional color(s). Color is an important property of a substance. The color of a material is associated with absorbance or reflectance. The human eye sees colors that complement that is absorbed[30].

3.8.4.SCANNING ELECTRON MICROSCOPY:

SEM is a versatile and advanced device mainly used for observation. Surface phenomenon of materials. The sample is irradiated with high-energy electrons by SEM, and the emitted electrons / X-rays are analyzed. These are coming Electron / X-rays are terrain, morphology, composition, Orientation of crystal grains of materials, crystallographic information, etc. form Shows shape and size, terrain shows surface features An object or "appearance", its texture, smoothness, or roughness. Likewise, composition means elements and compounds that constitute the material, while crystallography means the arrangement of atoms in the materials. SEM is the leading apparatus that is capable of achieving a detailed visual image of a particle with high quality and spatial resolution of 1 nm. Magnifications of this kind of apparatus can extend up to 300,000 times. Although SEM is used just to visualize surface images of a material and does not give any internal information, it is still considered as a powerful instrument that can be used in characterizing crystallographic, magnetic and electrical features of the sample and in determining if any morphological changes of the particle has occurred after modifying the sample surface with other molecules. SEM is able to provide several qualitative information of the specimen including its topography, morphology, composition and crystallographic information. others In other words, it has surface features and textures, shapes, sizes, and Arrangement of particles on the surface of the sample. With the nature of the element Compounds constituting the sample and their relative ratios and arrangements The number of atoms in a single crystal particle and their order can also be provided. Therefore, SEM is a versatile tool that can be investigated and analyzed. High resolution material[31].

Fig.3.14: SEM Instrument

SEM instruments are based on the principle that primary electrons are released of the source that powers the sample's atomic electrons then secondary electrons (SE) can be released and an image can be formed by collecting these secondary electrons at each point of the sample, the base requirement for SEM to operate in vacuum to avoid electronic interaction with gas molecules to obtain high

resolution. In addition, the main electrons generated and emitted by the electron gun are accelerated by heating or use high energy between 1 and 40 keV. These electrons are emitted focused and limited to a monochromatic beam (at 100 nm diameter or less) by magnetic lenses and metal slits in the vacuum column. Primary electrons are scanned across the surface of the sample by scanning coils in the frame model. The primary electron beam reaches the sample surface, it will interact with an area close to the sample surface at a given depth in different ways. The incident electrons are accelerated towards samples with the amount of kinetic energy they lose inside the sample by creating some signal from the interaction of electrons with the specimen.It scattered two elastic and inelastic in the sample[31].

3.9. CONCLUSION:

Methodology is a very important part of creating a good thin film. Choosing the right material and treating it the right way to create a thin film plays an important role. This chapter details the materials used in this process and how to use the atomizer spray pyrolysis process. The complete method of preparing the , cleaning the glass substrate, and coating the glass substrate is explained in the photo. The step-by-step process is clearly explained for better understanding.

CHAPTER-4

RESULTS AND DISCUSSION

4.1.INTRODUCTION:

This chapter described the results of coated Mg/TiO_2. The XRD, FTIR, thickness measurements, SEM images, EDX and its optical properties, (UV-Vis Spectroscopy) are clearly discussed in this chapter. The corresponding figures and tables are shown.

4.2. XRD ANALYSIS:

The XRD Spectra was observed for coated Mg/TiO_2 on the TCO substrates.It was observed on different types of TCO substrates and commercially available FTO. The XRD measurements were recorded to analyse the structural parameters such as crystal structure,grain size, microstrain etc. The graph is plotted and the peaks are observed at different miller planes. The Mg/TiO_2 substrates are annealed at 350 ℃ for 3 hours. XRD table for different molarities is tabulated and their spectra is provided below. These values are compared with the JCPDS (Joint Committee on the Powder Diffraction Spectra Data) card number. High purity and crystallinity of the synthesized TiO_2 is revealed by the appearance of the clear and the sharp peaks.[66]. No change of the crystal structure on the doping process causes high intensity and a sharp anatase peaks which enhances the crystallinity of the anatase phase. Absence of the magnesium peak attributed low metal ion dopant content as well as appropriate dispersion of metal ion deposits on TiO_2 nanoparticles[71]. The observed mixed phases of anatase and rutile TiO_2 were due to the influence of Mg dopant in the formation of TiO_2 crystals. Mg doped TiO_2 polyscales indicated that the increase in peak intensities results in inducing well crystalline phases which are apparently stable and also enhances the photochemical activities[17]. As Mg^{2+} is more electropositive, the electronic cloud in each TiO_2 might be loosely held, favoring the formation of the less dense anatase phase[16]. No visible peaks for Mg confirmed that it was completely doped in TiO_2. It is found that phases of TiO_2 are strongly dependent on coating layer. Mg dopant in the TiO_2 is responsible for the change of the phases of TiO_2 compound. It may be attributed to the smaller atomic size of Mg, which affects the force constant and amplitude of vibration of the nearest bands. These mixed phases of TiO_2 are expected to enhance the optoelectronic activity of TiO_2. All the coated films have high peak intensity which refers to good crystalline phases of TiO_2 that improves the phototchemical activities[62].

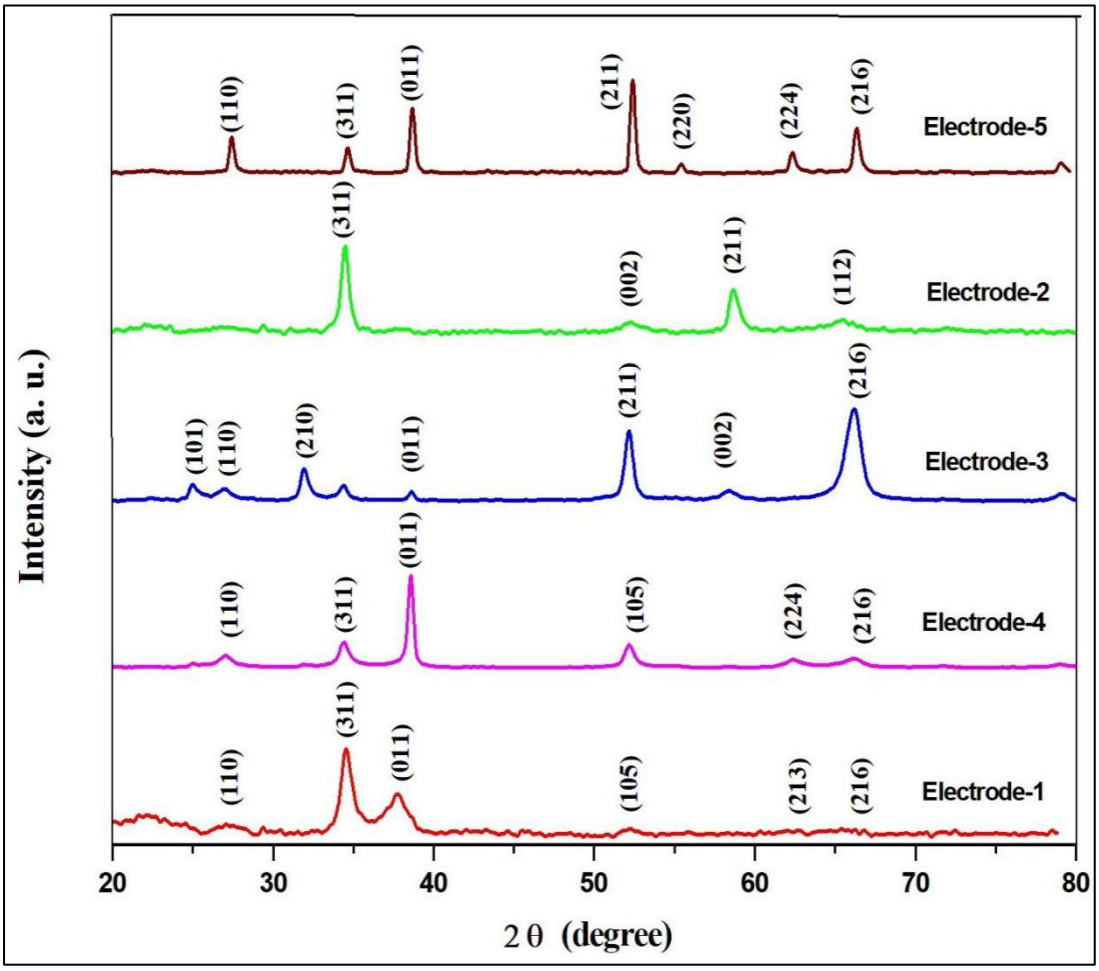

Fig.4.1: XRD patterns of various electrodes

COMPARISON WITH JCPDS CARD:

TABLE: 4.1: COMPARISON WITH JCPDS CARD:

S.NO.	***NAME OF THE ELECTRODES***	***2θ***	***hkl***
1	Electrode-1 (ZTO 1-Mg/TiO_2)	27.37	110[33]
		34.65	311[36]
		38.75	011[33]
		52.44	105[16]
		62.39	213[37]
		66.29	216[37]
2	Electrode-2 (ZTO 2-Mg/TiO_2)	34.64	311[36]
		58.79	211[16]
		52.53	002[38]
		65.64	112[38]

3	Electrode-3 (TO 1-Mg/TiO_2)	25.17	101[16]
		27.31	110[33]
		32.01	210[35]
		34.56	210[35]
		38.66	011[33]
		52.34	211[16]
		58.40	002[38]
		66.42	216[37]
4	Electrode-4 (TO 2-Mg/TiO_2)	27.12	110[33]
		34.56	311[36]
		38.46	004[16]
		52.34	105[34]
		62.51	224[35]
		66.22	216[37]
5	Electrode-5 (FTO-Mg/TiO_2)	27.31	110[33]
		34.56	311[36]
		38.85	011[33]
		52.53	211[16]
		55.66	220[38]
		62.51	224[35]
		66.42	216[37]

The XRD pattern of electrodes synthesized by spray pyrolysis and annealed at 350℃ for 45 mins is given in fig 4.1. The diffraction pattern shows the anatase form of the titanium.The spectrum is plotted between the intensity and the 2θ degree value. The prominent diffraction peaks of electrode-1 shows the presence of magnesium compounds at 34.65º (311) and Mg/TiO_2 prominent peak at 38.75º (011). For the electrode-2 the magnesium compound peak is present at 34.56º (311) and the other peak at 58.79º which has a hkl value of (002) is the tetragonal structure of tin.

For the electrode-3 the Mg/TiO_2 prominent peak is at 66.42º which has a hkl value of (216). The electrode-4 the Mg/TiO_2 has prominent peak at 38.46º with a hkl value of (004), the titanium peak at 34.56º is (210) plane and a peak at 52.34º belongs to (105) plane.

For the electrode-5, the prominent peak is present at 52.53º with hkl value of (105). The peak at 38.85º has a hkl value of (011). The anatase peak of titanium is at 66.42º with a hkl value of (216). The peak of Mg/TiO_2 crystalline structure is at 27.31º with a hkl value (110). The above mentioned intensities and diffraction planes confirm the formation of Mg/TiO_2.

When we compare with Electrode 1 and Electrode 2 it is well known that the expected phase is mostly found in Electrode 1.It is due to the reactions between the magnesium and titanium. On comparing the electrode-3 and electrode -4 it is known that the expected phases are mostly found in the electrode-3. This may be due to the less molarity of TCO substrate or due to the recombination of the TCO and the phototanode layer. When electrode-5 compared with all other electrodes as it was commercially bought it has the expected phases as the Mg/TiO_2 coated substrates. This may be due to the recombination between the two layers.

4.3.GRAIN SIZE,MICROSTRAIN AND DISLOCATION DENSITY:

By using the XRD results the Grain Size, Microstrain and the Dislocation density of the coated substrates can be found. They are calculated using the formula provided below and their values are tabulated.

GRAIN SIZE:

The grain size or crystalline size was calculated using the equation Debye Scherrer formula. It depends upon the Full Width Half Maximum and the angle of the peak. It is named after Paul Scherrer. The grain size of the coated glass substrate can be calculated using the formula

$$D=K\lambda/\beta \cos\theta$$

Where , K is the dimensionless shape factor, whose value is 0.9.

λ is the wavelenght of Kα radiation =0.15406 nm

β is the Full Width Half Maximum values of the peaks in XRD Data

Cos θ is the Bragg's Angle

MICROSTRAIN:

The microstrain can be calculated using the formula

$$\varepsilon=\beta \cos\theta/4$$

Where , β is the Full Width Half Maximum values of the peaks in XRD data

Cos θ is the Bragg's Angle.

DISLOCATION DENSITY:

The dislocation density can be calculated using the formula

$$S=1/D^2 (nm)^2$$

Where , D is the Grain Size values.

TABLE:4.2 : GRAIN SIZE AND MOLARITY

MOLARITY	*NAME OF THE ELECTRODES*	*GRAIN SIZE (nm)*	*MICROSTRAIN (10^{-6})*
0.05M	Mg/Tio2 - Electrode 1(ZTO-1)	18.5613 nm	0.0605249
0.15M	Mg/Tio2 - Electrode 2(ZTO-2)	25.98 nm	0.0432213
0.3M	Mg/Tio2 - Electrode 3(SnO_2-1)	13.48 nm	0.175943
0.4M	Mg/Tio2 - Electrode 4(SnO_2-2)	75.25 nm	0.0170909
COMMERCIAL	Mg/Tio2 - Electrode 5(FTO)	110.77 nm	0.0161397

From the above table, it is clearly seen that the Grain Size increases when the Mg/TiO_2 substrates are annealed at 350℃. The grain size depends on the annealing temperature and the time. If the thin film is annealed at a high temperature with an increase in the time the Grain size increases. But, the microstrain decreases due to the annealing process. These properties increases the ductility of the materials with an decrease in hardness.

TABLE:4.3: DISLOCATION DENSITY

TCO'S USED	*MATERIALS*	*DISLOCATION DENSITY (10^{14}) (nm^{-2})*
ZTO-1	Mg/TiO_2 electrode-1	29.02
ZTO-2	Mg/TiO_2 electrode-2	14.81
TO-1	Mg/TiO_2 electrode-3	54.95
TO-2	Mg/TiO_2 electrode-4	1.76
FTO	Mg/TiO_2 electrode-5	0.81

From the above table, it is understood that dislocation density is inversely proportional to the grain size. This is due to the reduction of lattice defects and improved crystal structurewith increase in crystalline size.

4.4. FESEM ANALYSIS:

The morphological parameters of $MgTiO_2$ thin films deposited on the TCO substrates were analysed using a field emission scanning electron microscope (FESEM). The FESEM image shows that the surface morphology is strongly influenced by the volume of the precursor solution. The magnification range is of 100 nm. The FESEM images of coated Mg/TiO_2 layers are given below. It shows an average grain size of about 50 nm to 60 nm.

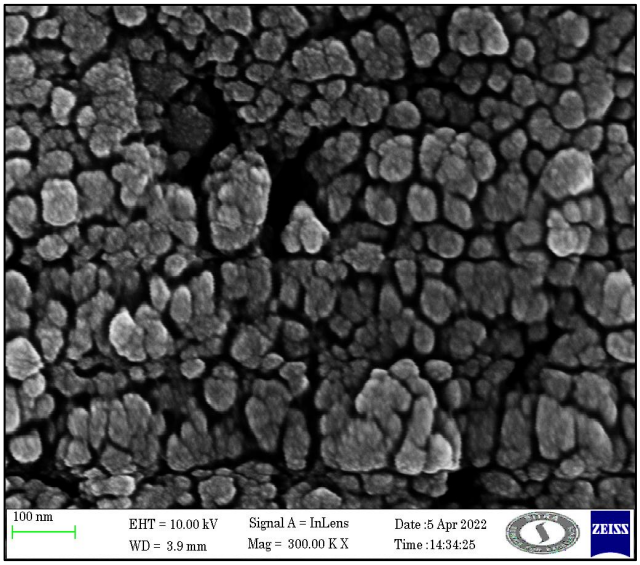

FIG.4.2: FESEM image of Electrode-1

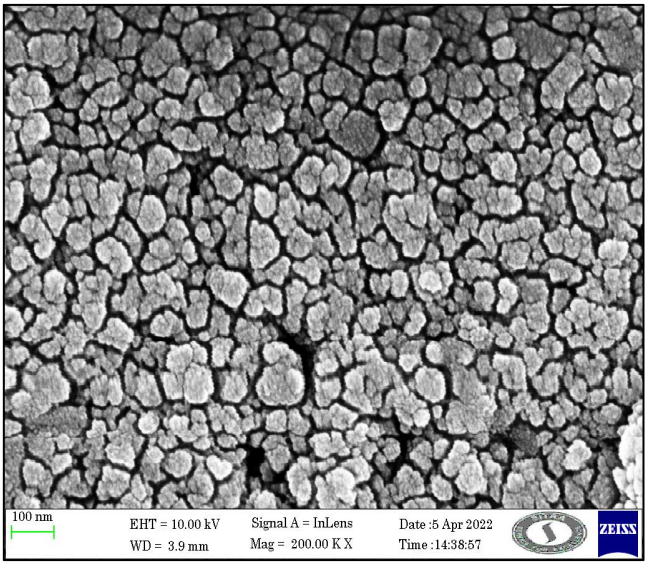

FIG.4.3:FESEM image of Electrode-2

FIG.4.4: FESEM image of Electrode-3

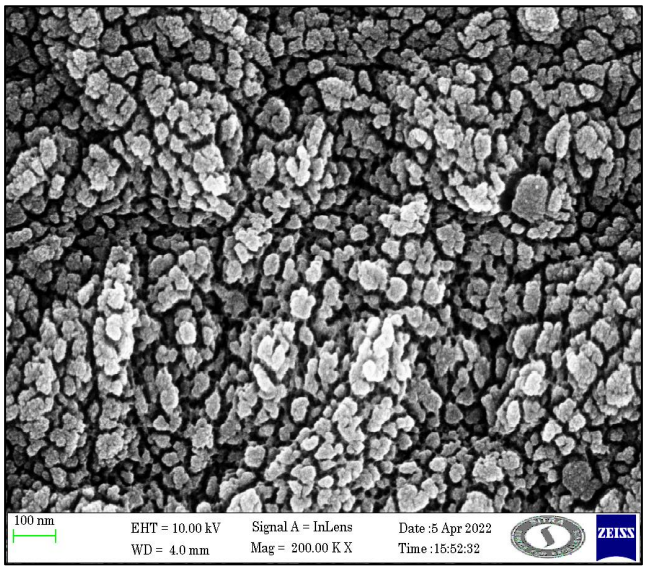

FIG.4.5: FESEM image of Electrode-4

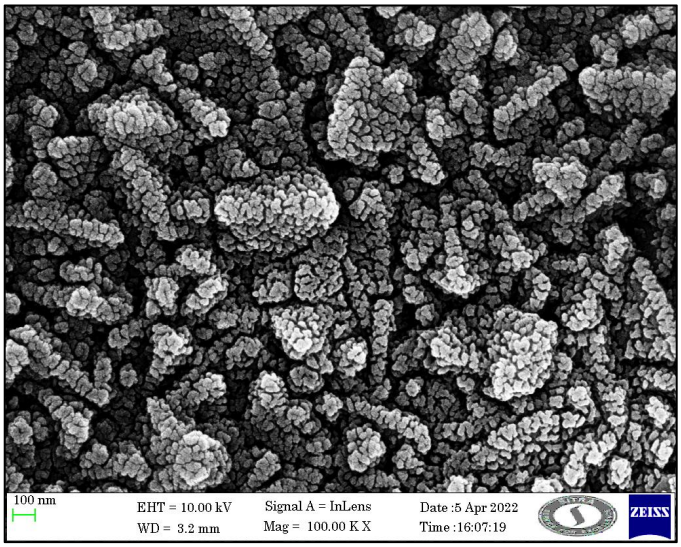

FIG.4.6: FESEM image of Electrode-5

The above figures gives the detailed image of the Mg/TiO_2 layer coated on the TCO substrates annealed at 350℃, which is studied from the FESEM analysis. It is evident that the grain size are arranged closely and compactly. The small and large grains are observed due to the grain growth. The thickness of the fabricated photoanodes of electrode-1,2,3,4 and 5 are 536.19 nm, 670.25nm,469.16nm,737.26nm and 335.12nm respectively. The Mg Doped TiO_2 shows a spherical crystal structure creating a high surface area and porosity quite suitable for enhancing photocatalytic activities[17]. As the molarity of the TCO increases the grain size is increased. It is because when the concentration increases the thickness increases which results in the increase in the grain size. On the annealing process the roughness of the film increases which increases the grain size.

4.5. EDAX ANALYSIS:

The presence of elements and the elements purity is observed by Energy Dispersive X-ray Spectroscopy. The EDAX spectrum of Mg/TiO_2 substrates are shown below. The EDAX results confirmed the presence of the Magnesium and Titanium on the TCO substrates. The highest peaks are obtained for Sn and O. Other than that, the peaks of Magnesium,Titanium and Zinc are observed. The unassigned peaks belong to the impurities present in the substrates.

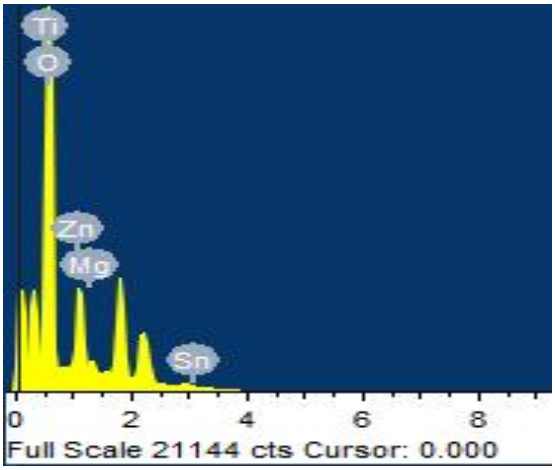

Element	Weight%
O K	95.52
Mg K	4.30
Ti K	0.02
Zn K	0.01
Sn L	0.15
Totals	100.00

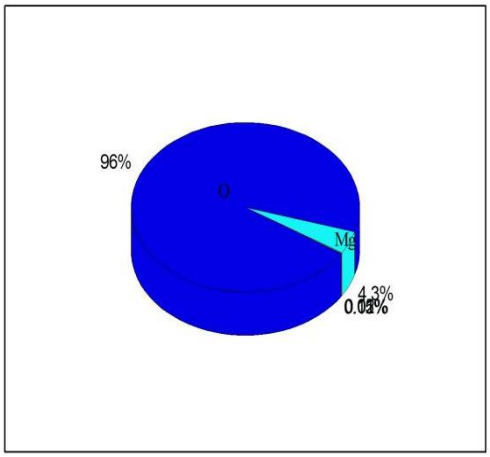

Fig .4.7: EDX image of the electrode -1

The above peak shows the presence of atmospheric oxygen, magnesium, tin, zinc and titanium. Here the oxygen peak is prominent due to the film coating in the open atmosphere. The weightage of oxygen is about 95.52%. The next peak of magnesium weight about 4.30%. The weight of Titanium is found to be about 0.02%.

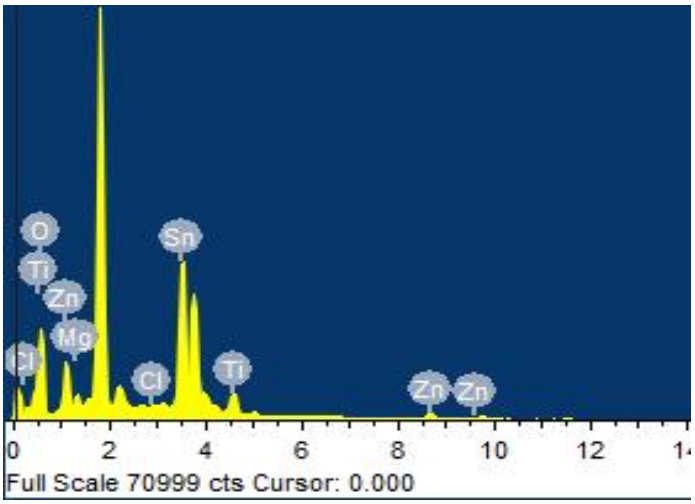

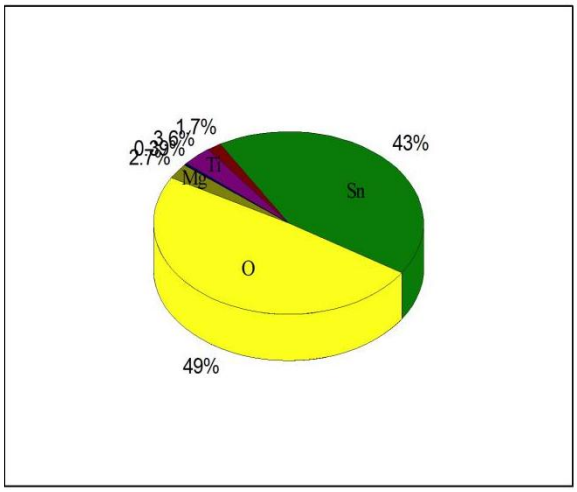

Element	Weight%
O K	49.05
Mg K	2.69
Cl K	0.39
Ti K	3.56
Zn K	1.69
Sn L	42.61
Totals	100.00

Fig.4.8: EDX image of the electrode-2

From the above FESEM chart, it is clear that the oxygen content is more prominent due to the open air coating. The next predominant peak corresponds to Sn. Magnesium content is analysed as 2.7%. And the Titanium is found to be about 3.5%. Here the chlorine peak is observed due to the TCO material used. The oxygen weightage is more due to the fabrication done in open space.

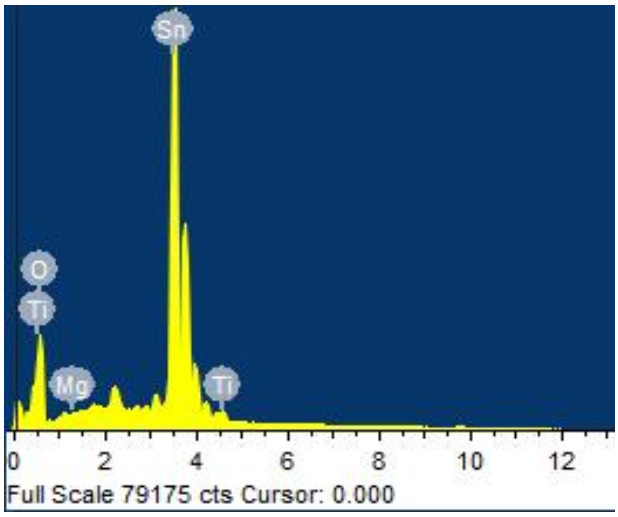

Element	Weight%
O K	0.02
Mg K	1.00
Ti K	31.20
Sn L	67.79
Totals	100.00

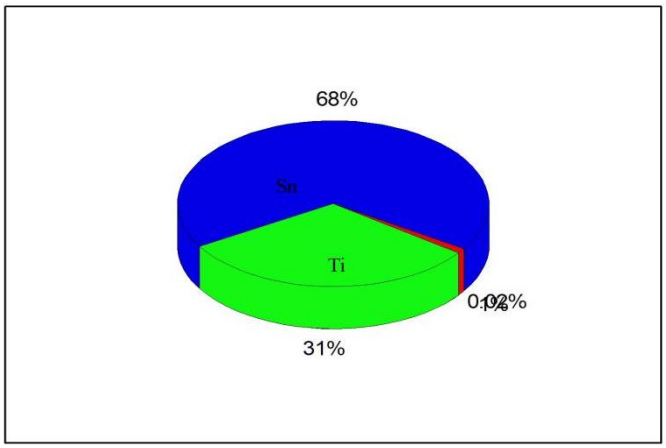

Fig.4.9. EDAX image of electrode-3

From the above EDAX image, it is observed that the peak for Sn is the prominent and the next peak observed was corresponding to the Titanium which is about 31%. The peak of magnesium is weighted to be 1%.There is no other compounds are observed in this electrode.

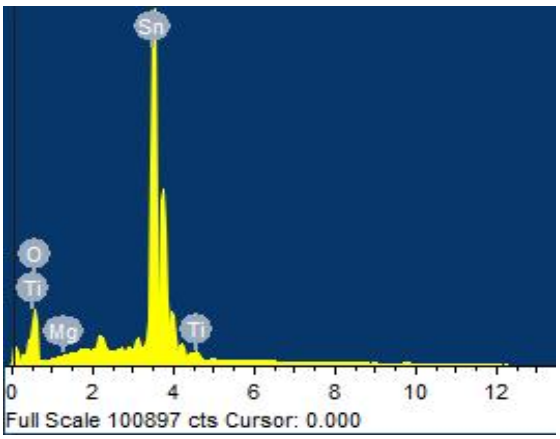

Element	Weight %
O K	1.03
Mg K	0.04
Ti K	37.58
Sn L	61.35
Totals	100.00

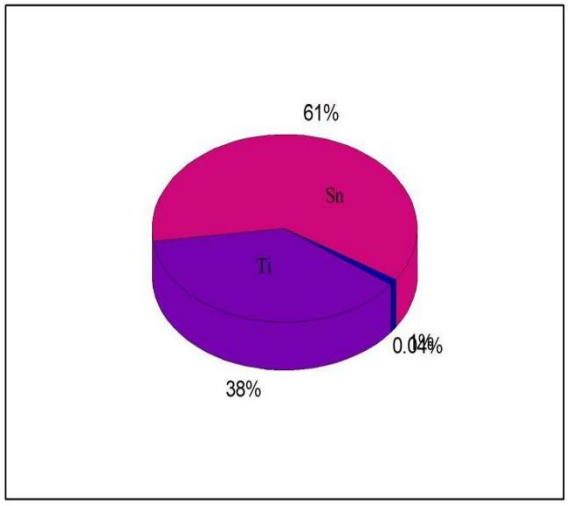

Fig.4.10: EDAX image of electrode-4

From the EDAX image of the electrode-4, it is seen that the peak is prominent for the Sn which is about 61%. The next peak corresponds to the Titanium which weights about 37%. The peak of Magnesium is found to be about 0.04% .

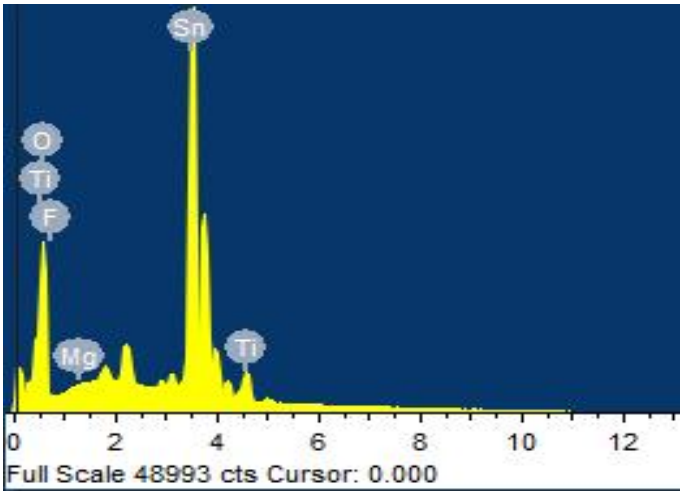

Element	Weight%
O K	48.22
F K	0.21
Mg K	0.03
Ti K	2.48
Sn L	49.06
Totals	100.00

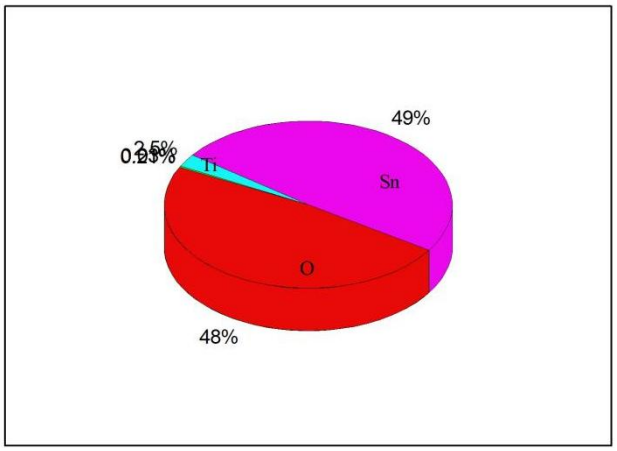

Fig.4.11: EDAX image of electrode-5

From the electrode-5 EDAX image, it is clearly seen that the prominent peak is Sn and the next peak corresponds to Oxygen. The weight of Titanium is about 2.4% and Magnesium is about 0.03%. From the all EDAX electrodes image, it is seen that the prominent peak maximum is obtained by Sn, this may be due to the recombination occuring on the coating process. Hence the Sn dominates the electrode materials used such as Magnesium and Titanium. From the EDAX results, we confirm that all the parent elements used for the electrode coatings are found.

4.6.FTIR ANALYSIS:

To understand the nature of Mg/TiO_2 FTIR spectra was recorded. It is observed for the substrates that were annealed at 350℃for 45 mins. Their graph is observed and explained below.

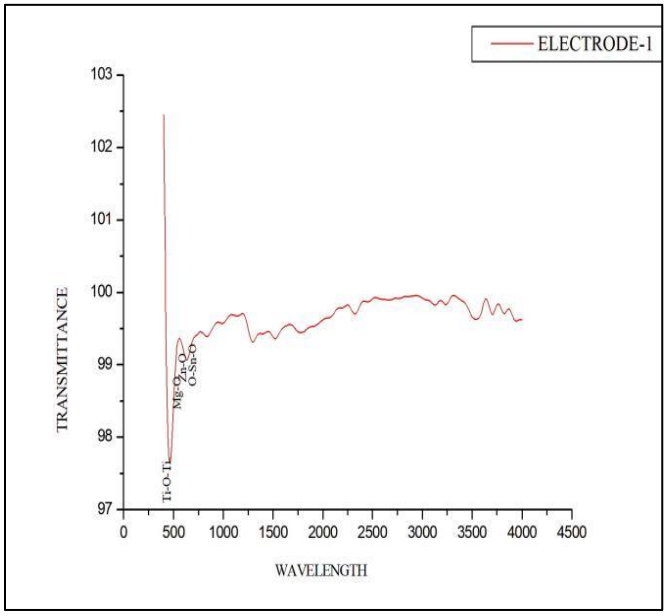

FIG.4.12: FTIR spectra of Electrode-1

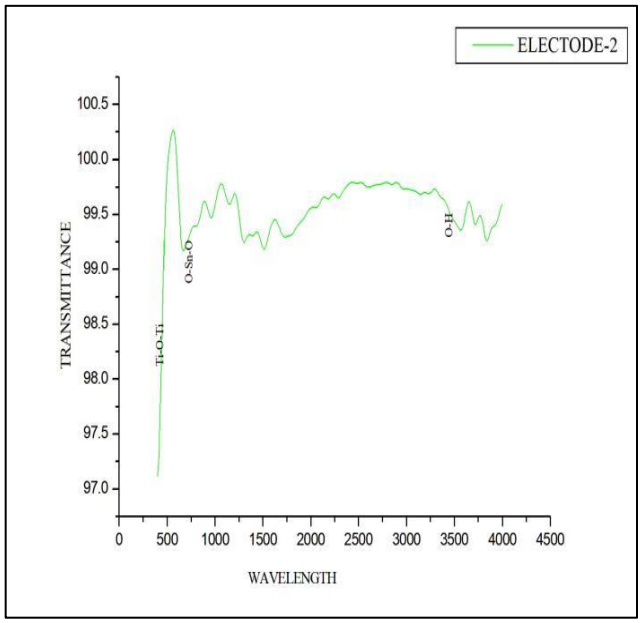

FIG.4.13: FTIR spectra of Electrode-2

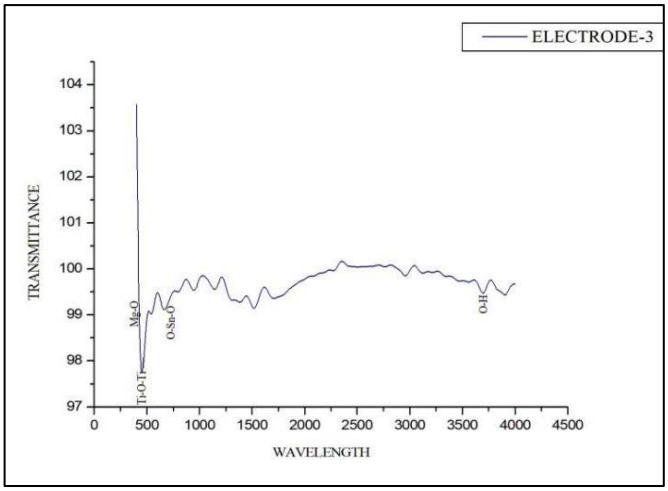

FIG.4.14: FTIR spectra of Electrode-3

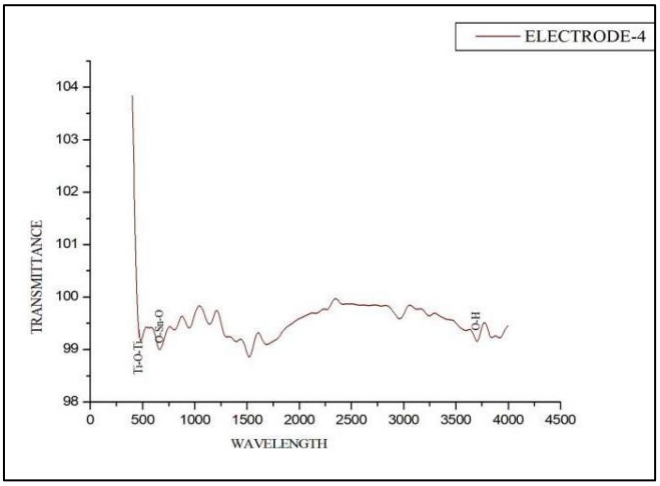

FIG.4.15: FTIR spectra of Electrode-4

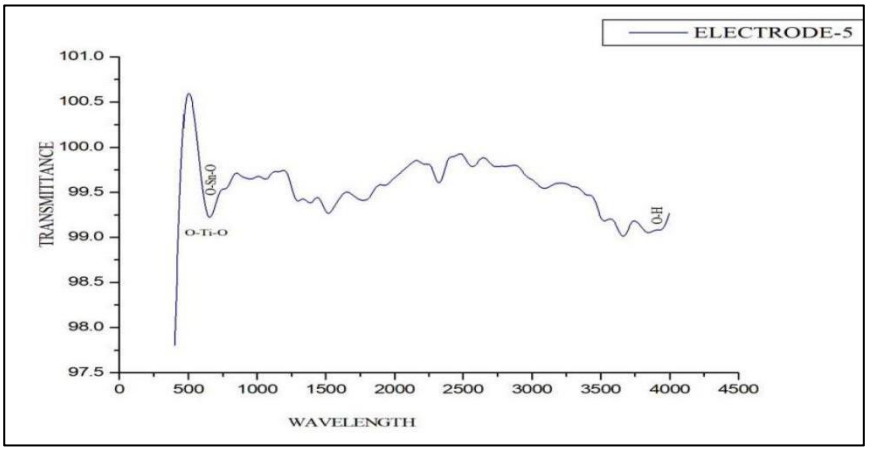

FIG.4.16: FTIR spectra of Electrode-5

The above figure represents the FTIR spectra of the coated Mg/TiO_2 thin film. The FTIR spectra for the electrodes 1,2,3,4&5 are recorded and the results are analyzed. The O-H stretching is observed at the wavenumber of more than 3000 cm^{-1}. This band is due to the presence of O-H groups and absorbed water bound at the surface of the electrodes. In above figures the prominent peak is at 455.20 cm^{-1} corresponding to the Ti-O-Ti vibration. The strongest peak at 686.66 cm^{-1} is due to the O-Sn-O vibrations. The peaks from 3400-3750 cm^{-1} are due to the O-H bonds present in the atmosphere or absorbance of water molecules at the sample surface.

TABLE. 4.4: PEAK VALUES OF FTIR:

S.NO.	***NAME OF THE ELECTRODES***	***PEAK VALUE***	***OBSERVED VIBRATIONS***
1	Electrode-1 (ZTO-1-Mg/TiO_2)	416.62	Ti-O-Ti bending[41]
		455.20	Ti-O-Ti vibration[46]
		516.92	Mg-O stretching[36]
		555.50	Sn-OH stretching[42]
		648.08	Sn-O stretching[45]
		686.66	O-Sn-O vibration[40]
2	Electrode-2 (ZTO-2-Mg/TiO_2)	416.62	Ti-O-Ti bending[41]
		455.20	Ti-O-Ti vibration[46]
		624.94	Sn-O stretching[43]
		648.08	Sn-O stretching[45]
		686.66	O-Sn-O vibrations[40]

3	Electrode-3 (TO-1-Mg/TiO_2)	424.34	Mg-O vibrations [46]
		455.20	Ti-O-Ti vibration[46]
		532.35	Absorption of Zn-O bond [44]
		648.08	Sn-O stretching [45]
		686.66	O-Sn-O vibrations [40]
4	Electrode-4 (TO-2-Mg/TiO_2)	455.20	Ti-O-Ti vibration [46]
		617.22	Absorption bond of Sn-O-Sn [47]
		686.66	O-Sn-O vibrations[40]
5	Electrode-5 (FTO-Mg/TiO_2)	432.05	O-Ti-O bonding [48]
		686.66	O-Sn-O vibrations[40]

From the electrode-1,(figure 4.12), the peak at 555.50 cm^{-1} is due to the absorption of Zn-O stretching vibration. The peak at 516.92 cm^{-1} is due to the stretching vibration mode of Mg-O. The peak at 416.62 cm^{-1} corresponds to the bending vibrations of Ti-O-Ti. In the electrode-2 (figure 4.13), the peak at 624.94 cm^{-1} is due the Sn-O stretching vibration. The peak at 3448.72 cm^{-1} due to the O-H bonding. From the electrode-3(Fig.4.14) spectrum, the peak at 424.34 cm^{-1} is formed due to the vibration of Mg-O. The peak at 532.35 cm^{-1} is due to the absorption of Zn-O bonding. The peak at 648.08 cm^{-1} corresponding to the stretching vibrations of Sn-O. From the electrode-4 spectrum (Fig.4.15), the peak at 617.22 cm^{-1} is due to the absorption bands of Sn-O-Sn vibrations. The peak at 524.64 cm^{-1} is due to the Sn-OH stretching vibrations. From the FTIR spectrum of electrode -5 (Fig.4.16), the peak at 432.05 cm^{-1} is due to the O-Ti-O bonding.

4.7.THICKNESS MEASUREMENT:

The thickness of the coated Mg/TiO_2 films are calculated and are tabulated below. The thickness is calculated after the substrates are annealed at 350°C for 45 min. The weight of the glass substrate is noted before and after the coating process and the thickness is calculated. The thickness is calculated by using the formula

$$T=W/\rho A \ (m)$$

Where, W – difference in weight of substrates before and after coating

ρ - density of the materials

A – area of the coated substrate (0.25 cm^2)

TABLE:4.5 : THICKNESS

S.NO.	***NAME OF THE ELECTRODES***	***TCO SUBSTRATES***	***WEIGHT(gms)***		***THICKNESS*** (nm)
			BEFORE COATING	***AFTER COATING***	
1	Mg/TiO_2 electrode-1	ZTO-1	2.2964	2.2972	536.19
2	Mg/TiO_2 electrode-2	ZTO-2	1.9484	1.9494	670.25
3	Mg/TiO_2 electrode-3	SnO_2-1	2.0005	2.0012	469.16
4	Mg/TiO_2 electrode-4	SnO_2-2	1.8261	1.8272	737.26
5	Mg/TiO_2 electrode-5	FTO	1.2537	1.2587	335.12

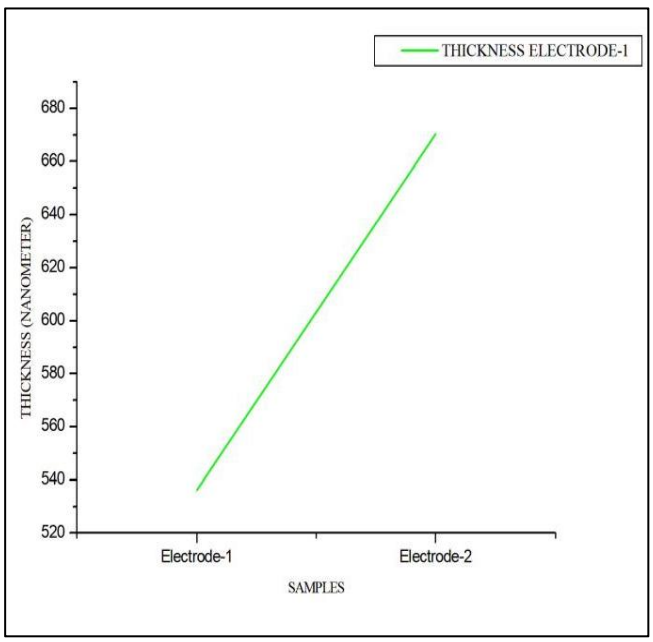

Fig.4.17: Thickness of the electrodes 1&2

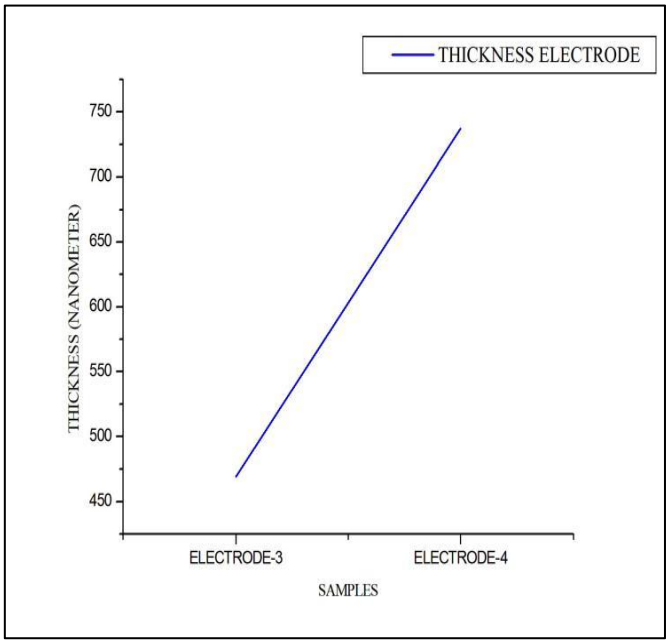

Fig.4.18: Thickness of the electrodes 3&4

The difference in thickness may arise due to the deposition technique, where there is a huge migration or dislocation of the grains. Secondly, it is evident from fig 4.17 & 4.18 that as the molarity of the compounds increase, the thickness of the Mg/TiO_2 layer increases respectively. This might have occurred due to the formation of the Mg/TiO_2 layer with the substrates during the spray pyrolysis process which depends on the concentration of the solution, or during the spraying duration. The may have the molecular interactions, which leads to condensed films. The roughness of the film changes upon theincrease in the TCO concentration. Moreover, a thin layer of Mg/TiO_2 layer is ideal for its application as a charge transport layer in solar cells. A thick layer Mg/TiO_2 layer can produce large

charge carrier as it can absorb more photons. But, a layer of very high thickness can result in charge recombination.

4.8.UV-VIS-NIR ANALYSIS:

The optical properties of the coated Mg/TiO_2 thin films are analysed by using the UV Spectroscopy. The absorbance and transmittance spectra are observed for different substrates. The transmittance and absorbance of $MgTiO_2$ coated on different TCO are compared and analysed.

✧ ***ABSORBANCE:***

The optical absorbance spectra of $MgTiO_2$ coated on different TCO substrates are given below.

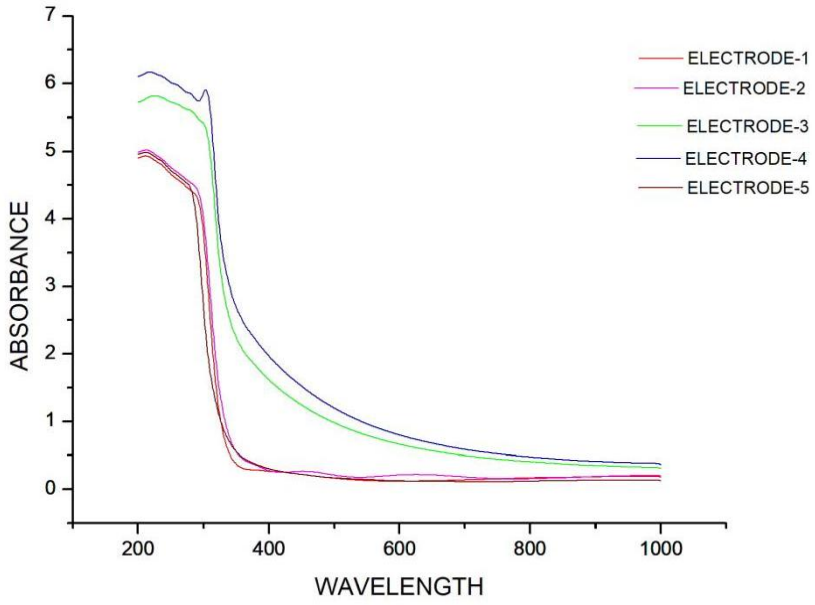

Fig.4.19: Absorbance spectra of Mg/TiO_2 substrates

From the fig 4.19, the optical absorbance is increased with the increase in each molarity of different TCO compounds. Absorption is enhanced,due to the increase in the Fermi energy of Mg and decrease in the bandgap which makes the electrons jump easily from the valence band to the conduction band.[16]. The electrode -4 has the highest absorbance among all the electrodes. The absorption of the sample increases with the concentration because the amount of dissolved molecules in the sample increases.

✧ ***BANDGAP:***

Band gap is calculated from Tauc plot, using plotted the wavelength and absorption values obtained from the UV analysis. The graph was plotted between the Energy and the $(\alpha h\nu)^2$ values in the x-axis and y-axis respectively. The samples were annealed at 350℃ for 45 mins. Here it is seen that for an increase in TCO substrate molarity, there is a decreases in bandgap.

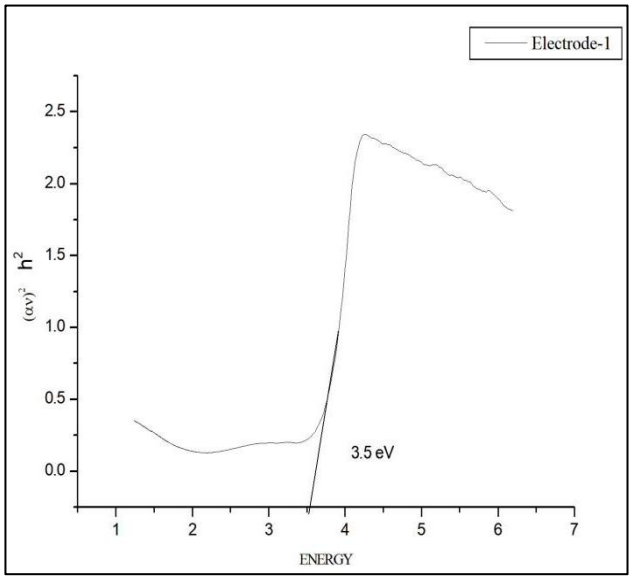

Fig.4.20: Band gap Of Electrode-1

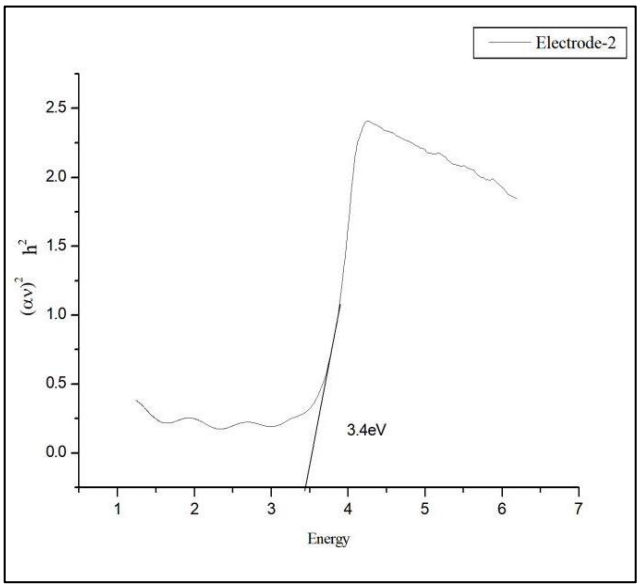

Fig.4.21: Band gap Of Electrode-2

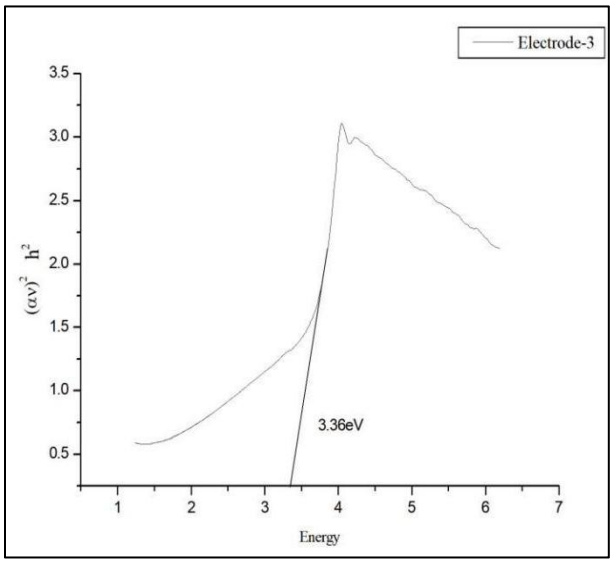

Fig.4.22: Band gap Of Electrode-3

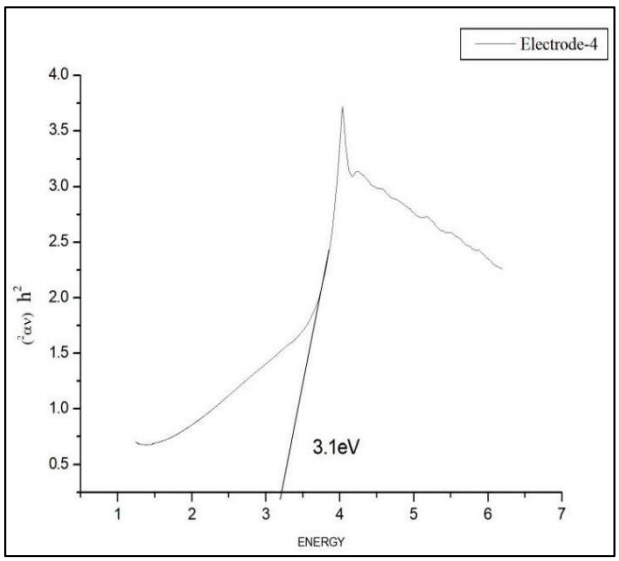

Fig.4.23: Band gap Of Electrode-4

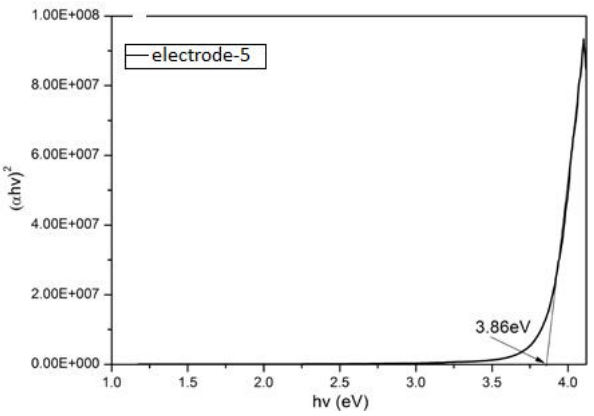

Fig.4.24:Band gap Of Electrode-5

From the above graphs, it is seen that the bandgap decrease as the molarity of the material is increased.The band gap lowering is attributed to the introduction of Mg^{2+} as an impurity into the TiO_2 , which creates extra energy levels inside the band gap. The extra energy level formed within the bandgap as the fermi energy level of Mg^{2+} shifts towards the valence band, resulting in a p-type semiconductor[17].

TABLE:4.6: BANDGAP

S. NO.	***NAME OF THE ELECTRODES***	***TCO***	***BANDGAP***
1	Mg/TiO_2 electrode-1	ZTO-1	3.5 eV
2	Mg/TiO_2 electrode-2	ZTO-2	3.4 eV
3	Mg/TiO_2 electrode-3	TO-1	3.21 eV
4	Mg/TiO_2 electrode-4	TO-2	3.19 eV
5	Mg/TiO_2 electrode-5	FTO	3.86 eV

TiO_2 has oxygen vacancies which is formed during the annealing. Adding dopant to the titanium creates a new energy level in the intermediate positions due to the injection of the impurities within the lattice or crystal structure. Reduction in the bandgap is due to the creation of new energy levels due to the addition of magnesium. Here the addition of magnesium into the TiO_2 has decreased in the bandgap values[2]. This is due the following four reasons 1) The exchange interactions 2) The carrier impurity interaction which affect the majority carrier band. 3) The carrier-carrier or electron- hole interaction 4) carrier impurity interaction which affect the minority carrier band[73].

✧ ***TRANSMITTANCE:***

The optical transmittance is essential for evaluating the optical performance of the Mg/TiO_2 thin films. The values are found by the UV-Vis NIR analysis. The transparency in visible region is required for optoelectronic devices. The graph is plotted between the transmittance and the wavelength in the x-axis and y-axis respectively. The samples were annealed at 350℃ for 45 min.

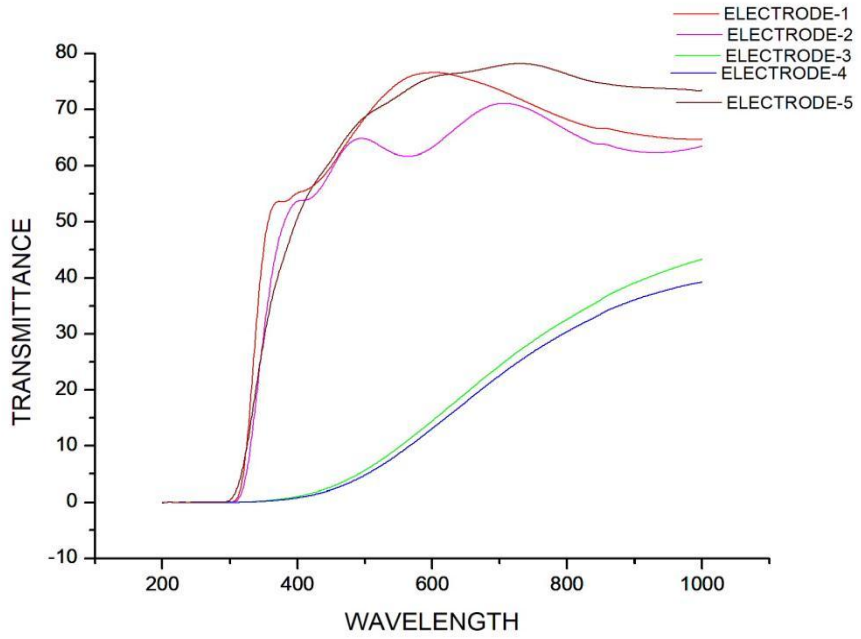

Fig.4.25: Transmittance spectra of the Electrodes

From Fig 4.24, the transmittance value for the different materials at different molar ratios are calculated and are provided in table 4.7.

TABLE:4.7: TRANSMITTANCE

S.NO.	***MATERIAL WITH Mg DOPED INTO TiO_2 COATED ON TCO***	***TCO***	***TRANSMITTANCE IN %***
1	Mg/TiO_2 electrode-1	ZTO-1	64%
2	Mg/TiO_2 electrode-2	ZTO-2	63%
3	Mg/TiO_2 electrode-3	TO-1	43%
4	Mg/TiO_2 electrode-4	TO-2	39%
5	Mg/TiO_2 electrode-5	FTO	73%

From the above table, it is seen that as the TCO molarity increases the transmittance of the film decreases in each material.Lower molar concentration causes increase in the transmittance. Increase in the wavelength causes increase in the transmittance. The thin film possess high transmittance in the visible and in the IR region. Transmittance decreases as the growth of grain increases and causes increase in scattering effect. The electrical conductivity increases as the optical transmittance increases.The transmittance decreases on doping the Mg into Titanium compared to the Transparent conducting oxides. This is due to the increase in the fermi energy levels and decrease in the band gap.

4.8.INFLUENCE OF MAGNESIUM IN TITANIUM:

A specific direction for photo-injected electrons in the TiO_2 conduction band is defined by inserting a Mg layer with a high conduction band edge between TiO_2 and the dye interface. Because charge recombination is delayed in photoanodes, the electron lifetime is improved. The opencircuit photo voltage decline as a function of time was used to investigate electron recombination kinetics. When the illumination is switched off in an open-circuit scenario, the electron density in the conduction band of TiO_2 begins to fall due to electron recombination, resulting in V_{oc} decay.The improved J_{SC} value can be attributed to an increase in the electron collection efficiency as a result of the increased photo injected electron lifetime[66].

4.8.1.INFLUENCE OF MAGNESIUM IN THE BAND GAP AND ABSORPTION :

Mg-doped TiO_2 polyscales have a high absorption band at 200-380, which is near the UV area. Broad absorption edges were seen in Mg-doped TiO_2 polyscales at 211 nm, which is within the visible spectrum of light. The optical absorption edges of Mg-doped TiO_2 polyscales revealed significantly shifted edges toward visible spectrum of light.The absorption edge shift to lower photon energy suggests a lower energy level in the conduction band, and so a shrinking band gap energy. Doping Mg into TiO_2 induces the apparent activation of Mg-doped TiO_2 polyscales under natural sunlight illumination that consists of 90% visible and 10% UV spectrum of light, respectively, after doping Mg into the TiO_2 crystalline system.The bandgap lowering can be attributed to the introduction of Mg^{2+} as an impurity into the host structure (TiO_2), which creates extra energy levels inside the bandgap. The extra energy level formed within the bandgap as the Fermi energy level of Mg^{2+} shifts towards the valence band, resulting in a P-type semiconductor[17].

Due to the injection of contaminants within the band-gap coupled with the production of oxygen vacancies by metal ion doping, new energy levels are produced at intermediate places by adding dopant, contributing to the strongly observed visible light absorption of Mg doped TiO_2 thin film. The formation of new energy levels due to the addition of Mg is credited with the reduction in band gap. These findings support that alkaline metal increases the photocatalytic activity of parent atoms when doped into TiO_2. The symmetry and flaws of the lattice are also altered, resulting in an increase in absorption. When Mg^{2+} is added to the structure, the atoms are rearranged into their proper lattice locations. As a result, the band gap shifts and electrical characteristics change.Oxygen vacancies are produced as a result of the Mg dopant, which are directly related to photon absorption and transportation into the final structure. When Mg is doped, the band gap shrinks, causing its absorption to shift towards the visible range. All of these changes in absorption and band gap tuning are linked to the availability of intermediate electron transport sources.[2].

Adding magnesium acetate tetrahydrate to the commonly used compact TiO_2 solution, which had tetrabutyl titanate as its main component in the isopropanol solution. Tetrabutyl titanate would hydrolyze promptly after a modest amount of magnesium acetate tetrahydrate was added, leaving a compact layer full of pores and agglomerated particles.The energy band broadens when Mg is doped into TiO_2, displacing the bottom of the conduction band up and the top of the valence band down.Mg-doping improves incident photon to current efficiency mostly in the short wavelength region, which should be attributed to improved light transmission in the corresponding wavelength range and improved cell charge transfer[18].

THERMAL STABILITY:

When Mg is doped into TiO_2, the crystalinity increases, as seen by XRD data, making it more stable at high temperatures and reducing weight loss. Because Mg dopant lowers the crystallisation temperature, its production requires less energy[2].

4.9. FOUR POINT PROBE ANALYSIS:

The variation in resistivity of Mg : TiO2 effects on electrical properties of films. Following relation is used to measure the sheet resistivity of films

$$\mathbf{R_S=(\pi/\ln 2)*(V/I)\ \Omega\ Cm}$$

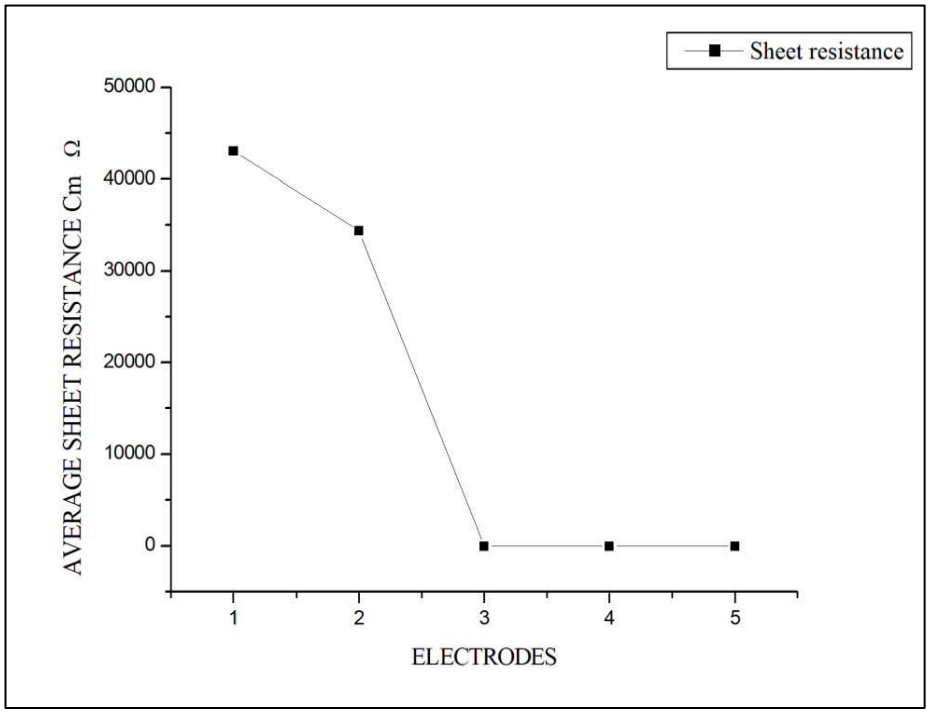

Fig.4.26: Sheet resistance graph

TABLE 4.8:SHEET RESISTANCE:

NAME OF THE ELECTRODES TCO-Mg/TiO_2	***SHEET RESISTANCE R_S(Ω Cm)***
Electrode-1(ZTO-1)	$4.3058*10^{4}$
Electrode-2(ZTO-2)	$3.438*10^{4}$
Electrode-3(SnO_2-1)	$467.425*10^{-17}$
Electrode-4(SnO_2-2)	$695.059*10^{-7}$
Electrode-5(FTO)	$577.224*10^{-17}$

The doping of Mg^{2+} atoms into the TiO_2 structure is responsible for the decrease in resistivity. The electron density has increased as a result of the decrease in resistance. Furthermore, when the thickness increases, the concentration of electrons increases, causing the resistivity to decrease[62].

4.10. CONCLUSION:

From this chapter the results of XRD,FTIR,FESEM, EDX,ABSORPTION,TRANSMITTANCE were taken and their results were discussed. From the XRD, we have calculated the grain size, microstrain etc. The grain size is increased for the increase in the molarity of the TCO used. The grain size is improved that indicates the better crystal. The absorption increases compared to TCO on doping Mg into TiO_2 as it creates a fermi energy level and the band gap decrease as it increases the transmittance.

CHAPTER-5

SUMMARY AND CONCLUSION

Sun is a natural source for the solar energy. The light from the sun is absorbed and converted into electricity by photovoltaic principle. The solar cells is of three generations and they are discussed in the above chapters. To increase the efficiency we here coat the Mg/TiO_2 layer into the TCO substrates of different molarity.

The solution is prepared by adding 0.1 M molar ratio of Magnesium Acetate Tetrahydrate to the 6 ml of Titanium Isopropoxide and 50 ml of isopropanol and stirred until the salt is dissolved. Then the solution is coated on the TCO substrates at 400℃ by the spray pyrolysis method and then annealed for 350℃ for 45 mins.Here we have taken the electrodes(photoanodes) in the combination of magnesium and titanium.

In this work, we have studied about the influence caused by magnesium doped into titanium. The XRD results revealed that the grain size is increased as the concentration of the TCO substrates increases. From the XRD we have calculated the grain size, microstrain and the dislocation density. The FESEM result confirms the morphology of the coated layer as the spherical structure. The EDAX results revealed that the presence of the compounds used, the Sn is the prominent peak in the electrodes this may be due to the recombination caused during the coating process. In the FTIR analysis shows the presence of the compounds used. The thickness of the coated Mg/TiO_2 is measured by the weight noted before and after coating, the thickness increases with the increase in the TCO molarity. This may be due to the interaction of Mg/TiO_2 coated layer with the TCO substrates during the deposition process. From the UV-Vis Spectroscopy the absorbance ,band gap,transmittance are discussed. The absorbance of the Mg/TiO_2 is increased compared to the TCO substrates. This is due to the increase in the fermi energy level of Mg. The band gap is decreased due to the addition of Mg , as it creates a new energy level in intermediate position, which makes the electrons to jump easily from the valence band to the conduction band. The transmittance is decreased as the absorbance is increased. The sheet resistance is calculated from the four point probe analysis and are tabulated in the previous chapters.

REFERENCES:

1. - De Bastiani, Michele 2016/03/09 Ph.D. Thesis: The stability of third generation solar cells
2. Zafar Arshad, Asif Hussain Khoja, Sehar Shakir, Asif Afzal, M.A. Mujtaba, Manzoore Elahi M. Soudagar, H. Fayaz, Ahamed Saleel C, Sarah Farukh, Mudassar Saeed,Magnesium doped TiO2 as an efficient electron transport layer in perovskite solar cells,Case Studies in Thermal Engineering,Volume 26,2021,101101,ISSN 2214-157X,https://doi.org/10.1016/j.csite.2021.101101
3. Tang, H., He, S. & Peng, C. A Short Progress Report on High-Efficiency Perovskite Solar Cells. *Nanoscale Res Lett* **12,** 410 (2017). https://doi.org/10.1186/s11671-017-2187-5
4. *Swaroop Kumar Mandal*; *Samarjeet Kumar*; *Purushottam Kumar Singh*; *Santosh Kumar Mishra* and *D.K. Singh*, (2020), Performance investigation of nanocomposite based solar water heater, *Energy*, **198**, ©
5. Rashmi A. Despande Advances In Solar Cell Technology: an overview volume 65, Issue 2, 2021 Journal of Scientific Research
6. Paul Hersch, Kenneth Zweibel -Basic photovoltaic principles and methods - February 1982
7. https://www.britannica.com/technology/solar-cell
8. https://www.energy.gov/eere/solar/solar-photovoltaic-cell-basics
9. Askari, Mohammad & Mirzaei Mahmoud Abadi, Vahid & Mirhabibi, Mohsen. (2015). Types of Solar Cells and Application. American Journal of Optics and Photonics. 3. 2015. 10.11648/j.ajop.20150305.17.
10. Rashmi Swami Solar Cell International Journal of Scientific and Research Publications, Volume 2, Issue 7, July 2012 1 ISSN 2250-3153
11. Shaikh, Mohd Rizwan & Shaikh, Sirajuddin & Waghmare, Santosh & Labade, Suvarna & Tekale, Anil. (2017). A Review Paper on Electricity Generation from Solar Energy. International Journal for Research in Applied Science and Engineering Technology. 887.
12. Askari, Mohammad & Mirzaei Mahmoud Abadi, Vahid & Mirhabibi, Mohsen. (2015). Types of Solar Cells and Application. American Journal of Optics and Photonics. 3. 2015. 10.11648/j.ajop.20150305.17
13. Afre, R., Sharma, N., Sharon, M. & Sharon, M. (2018). Transparent Conducting Oxide Films for Various Applications: A Review. REVIEWS ON ADVANCED MATERIALS SCIENCE, 53(1), 79-89 https://doi.org/10.1515/rams-2018-0006
14. https://www.lenntech.com/periodic/elements/ti.htm
15. https://www.toppr.com/guides/chemistry-formulas/magnesium-acetate-formula/

16. T. Siva Rao, Teshome Abdo Segne, T. Susmitha, A. Balaram Kiran, C. Subrahmanyam, "Photocatalytic Degradation of Dichlorvos in Visible Light by Mg2+ -TiO2 Nanocatalyst", Advances in Materials Science and Engineering, vol. 2012, Article ID 168780, 9 pages, 2012. https://doi.org/10.1155/2012/168780

17. Shivaraju, H.P., Midhun, G., Anil Kumar, K.M. *et al.* Degradation of selected industrial dyes using Mg-doped TiO2 polyscales under natural sun light as an alternative driving energy. *Appl Water Sci* **7,** 3937–3948 (2017). https://doi.org/10.1007/s13201-017-0546-0

18. Wang, Jing & Qin, Minchao & Tao, Hong & Ke, Weijun & Chen, Zhao & Wan, Jiawei & Qin, Pingli & Xiong, Liangbin & Hongwei, Lei & Yu, Huaqing & Fang, Guojia. (2015). Performance enhancement of perovskite solar cells with Mg-doped TiO2 compact film as the hole-blocking layer. Applied Physics Letters. 106. 121104. 10.1063/1.4916345.

19. Mantas Sriubas, Kristina Bočkutė, Darius Virbukas, Giedrius Laukaitis Investigation of the properties of Ca-doped TiO2 thin films formed by e-beam evaporation Procedia Engineering 98 (2014) 133 – 138

20. Sun T, Hao H, Hao WT, Yi SM, Li XP, Li JR. Preparation and antibacterial properties of titanium-doped ZnO from different zinc salts. Nanoscale Res Lett. 2014 Feb 27;9(1):98. doi: 10.1186/1556-276X-9-98. PMID: 24572014; PMCID: PMC4015756.

21. Yu, M., Sun, H., Huang, X., Yan, Y., & Zhang, W. (2020). In Situ-Formed and Low-Temperature-Deposited Nb:TiO2 Compact-Mesoporous Layer for Hysteresis-Less Perovskite Solar Cells with High Performance. *Nanoscale research letters*, *15*(1), 135. https://doi.org/10.1186/s11671-020-03366-1

22. Ali A. Yousif ,Kadhim A. Aadim and Nassar A. Hamzah Influence of Ag doping on Optical Properties of Nanocrystalline Titanium Dioxide prepared by PLD IOSR Journal of Applied Physics (IOSR-JAP) e-ISSN: 2278-4861.Volume 8, Issue 5 Ver. II (Sep - Oct. 2016), PP 50-56

23. Gaurav K. Upadhyaya , Vinod Kumara,b, L.P. Purohit Optimized CdO:TiO2 nanocomposites for heterojunction solar cell applications PII: S0925-8388(20)33817-2 DOI: https://doi.org/10.1016/j.jallcom.2020.157453 Reference: JALCOM 157453

24. Seshan, K. (2002). Handbook of thin film deposition techniques principles, methods, equipment and applications, second editon. CRC Press.

25. Jilani, Asim & Abdel-wahab, Mohamed & Hammad, Ahmed. (2017). Advance Deposition Techniques for Thin Film and Coating. 10.5772/65702

26. Vinay Kumar Singh Thin Film Deposition By Spray Pyrolysis Techniques Journal of Emerging Technologies and Innovative Research Journal of Emerging Technologies and Innovative Research volume 4 Issue 11 November 2017

27. Bunaciu AA, Udriştioiu EG, Aboul-Enein HY. X-ray diffraction: instrumentation and applications. Crit Rev Anal Chem. 2015;45(4):289-99. doi: 10.1080/10408347.2014.949616. PMID: 25831472.

28. Khan, Shahid & Khan, Sher & Khan, Latif & Farooq, Aliya & Akhtar, Kalsoom & Asiri, Abdullah M.. (2018). Fourier Transform Infrared Spectroscopy: Fundamentals and Application in Functional Groups and Nanomaterials Characterization. 10.1007/978-3-319-92955-2_9.

29. Alaa Frak Hussain UV-Visible Spectroscopt :https://www.researchgate.net/publication/337674152

30. Akhtar, Kalsoom & Khan, Shahid & Khan, Sher & Asiri, Abdullah M.. (2019). Scanning Electron Microscopy: Principle and Applications in Nanomaterials Characterization. 10.1007/978-3-319-92955-2_4.

31. https://pubchem.ncbi.nlm.nih.gov/compound/Magnesium-acetate-tetrahydrate

32. https://www.ebi.ac.uk/chebi/searchId.do?chebiId=CHEBI:139496

33. Shivaraju, H.P., Midhun, G., Anil Kumar, K.M. *et al.* Degradation of selected industrial dyes using Mg-doped TiO2 polyscales under natural sun light as an alternative driving energy. *Appl Water Sci* **7,** 3937–3948 (2017). https://doi.org/10.1007/s13201-017-0546-0

34. Qin, J., Zhang, Z., Shi, W. *et al.* The optimum titanium precursor of fabricating TiO2 compact layer for perovskite solar cells. *Nanoscale Res Lett* **12,** 640 (2017). https://doi.org/10.1186/s11671-017-2418-9.

35. Microwave Synthesis Titanium Doped Zinc Oxide for Solar Cell Application Vignesh P, Kanikairaj B Microwave Synthesis Titanium Doped Zinc Oxide for Solar Cell Application International Journal of Scientific Research in Science and Technology (IJSRST) Print ISSN : 2395-6011, Online ISSN : 2395-602X Volume 3, Issue 11, November-December-2017

36. Dhinasekaran, Durgalakshmi & Rakkesh, R. Ajay & Kamil, Syed & Karthikeyan, Subramani & Subrmanian, Balakumar. (2019). Rapid Dilapidation of Alcohol Using Magnesium Oxide and Magnesium Aspartate based Nanostructures: A Raman Spectroscopic and Molecular Simulation Approach. Journal of Inorganic and Organometallic Polymers and Materials. 29. 10.1007/s10904-019-01105-3.

37. S C, Vella Durai & E, Kumar & Muthuraj, D. (2021). Investigations on structural, optical, and impedance spectroscopy studies of titanium dioxide nanoparticles. Bulletin of the Chemical Society of Ethiopia. 35. 151-160. 10.4314/bcse.v35i1.13.

38. N. Shahzad , N. Ali , A. Shahid , S. Khan H. Alrobei Synthesis Of Tin Oxide Nanoparticles In Order To Study Its Properties Vol. 16, No. 1, January - March 2021, p. 41 - 49

39. Rina Sardiana Sari and Arif Rahman Hakim (2019) Bonding analysis of magnetic nanoparticles (MNPS) *zinc ferrite* (ZnFe2O4) encapsulated with silica (SIO2)IOP Conf. Ser.: Earth Environ. Sci. 382 012019

40. Premkumar, V. & Sivakumar, Ganesan. (2017). Hydrothermally synthesized cubic magnesium stannate (Mg2SnO4) nanoparticles and its electrochemical performances. Journal of Materials Science: Materials in Electronics. 28. 1-8. 10.1007/s10854-017-7280-0.

41. Roy, Soham & Tripathy, Nilakantha & Pradhan, Diana & Sahu, Prasanna & Kar, J.. (2018). Electrical characteristics of dip coated TiO 2 thin films with various withdrawal speeds for resistive switching applications. Applied Surface Science. 449. 10.1016/j.apsusc.2018.01.207

42. Farrukh, Muhammad Akhyar & Heng, B.-T & Adnan, Rohana. (2010). Surfactant-controlled aqueous synthesis of SnO2 nanoparticles via the hydrothermal and conventional heating methods. Turkish Journal of Chemistry. 34. 537-550. 10.3906/kim-1001-466

43. Babar, A. & Shinde, S.S. & Moholkar, Annasaheb & Rajpure, Keshav. (2010). Electrical and dielectric properties of co-precipitated nanocrystalline tin oxide. Journal of Alloys and Compounds - J ALLOYS COMPOUNDS. 505. 743-749. 10.1016/j.jallcom.2010.06.131.

44. Winiarski, Juliusz & Winiarska, Katarzyna & Szczygieł, Irena & Szczygieł, Bogdan. (2018). XPS and FT-IR Characterization of Selected Synthetic Corrosion Products of Zinc Expected in Neutral Environment Containing Chloride Ions. Journal of Spectroscopy. 2018. 1-14. 10.1155/2018/2079278.

45. Liu, Hui & Wang, An & Sun, Quan & Wang, Tingting & Zeng, He-Ping. (2017). Cu Nanoparticles/Fluorine-Doped Tin Oxide (FTO) Nanocomposites for Photocatalytic H 2 Evolution under Visible Light Irradiation. Catalysts. 7. 10.3390/catal7120385.

46. Sutapa, I.W., Wahab, A.W., Taba, P., & Nafie, N.L. (2018). Synthesis and Structural Profile Analysis of the MgO Nanoparticles Produced Through the Sol-Gel Method Followed by Annealing Process. Oriental journal of chemistry, 34, 1016-1025.

47. Samsonenko, Mariia & Zakutevskyy, Oleg & Khalameida, Svitlana & Charmas, B. & Skubiszewska-Zięba, Jadwiga. (2019). Influence of mechanochemical and microwave modification on ion-exchange properties of tin dioxide with respect to uranyl ions. Adsorption. 25. 10.1007/s10450-019-00036-2.

48. Chekin, F., Bagheri, S., & Abd Hamid, S.B. (2015). Synthesis and spectroscopic characterization of palladium-doped titanium dioxide catalyst. Bulletin of Materials Science, 38, 461-465.

49. Sameeksha Sharma , Nazilla Soleimanioun , Ravneet Kaur , Mamta Rani , S.K. Tripathi Comparative study of the effect of Mg, Zn and Ag dopants on properties of titanium dioxideas mesoporous ETL for photovoltaic application Materials Chemistry and Physics (IF4.094) Pub Date : 2021-01-01, DOI: 10.1016/j.matchemphys.2020.123730

50. M. Stefan, C. Leostean, D. Toloman, A. Popa, S. Macavei, A. Falamas, R. Suciu, L. Barbu-Tudoran, O. Marincas, O. Pana,New emerging magnetic, optical and photocatalytic

properties of Tb doped TiO2 interfaced with CoFe2O4 nanoparticles,Applied Surface Science,Volume 570,2021,151172,ISSN 0164332,https://doi.org/10.1016/j.apsusc.2021.151172.

51. Saint-André, Simón & Rodríguez, Daniel & Perillo, Patricia & Barrera, Marcela. (2021). TiO2 nanotubes antireflection coating design for GaAs solar cells. Solar Energy Materials and Solar Cells. 230. 111201. 10.1016/j.solmat.2021.111201.

52. Wei Huang, Jianhua Shi, Yiyang Liu, Zhuopeng Wu, Fanying Meng, Zhengxin Liu, High-performance Ti and W co-doped indium oxide films for silicon heterojunction solar cells prepared by reactive plasma deposition,Journal of Power Sources,Volume 506,2021,230101,ISSN 0378-7753,https://doi.org/10.1016/j.jpowsour.2021.230101.

53. Seyed Masoud Parsa, Alireza Yazdani, Hayder Dhahad, Wissam H. Alawee, Sadra Hesabi, Fatemeh Norozpour, Davoud Javadi Y, Hafiz Muhammad Ali, Masoud Afrand,Effect of Ag, Au, TiO2 metallic/metal oxide nanoparticles in double-slope solar stills via thermodynamic and environmental analysis,Journal of Cleaner Production,Volume 311,2021,127689,ISSN 0959-6526,https://doi.org/10.1016/j.jclepro.2021.127689

54. Dorow-Gerspach D, Mergel D, Wuttig M. Effects of Different Amounts of Nb Doping on Electrical, Optical and Structural Properties in Sputtered TiO_{2-x} Films. *Crystals*. 2021; 11(3):301. https://doi.org/10.3390/cryst11030301

55. S C, Vella Durai & E, Kumar & Muthuraj, D. (2021). Investigations on structural, optical, and impedance spectroscopy studies of titanium dioxide nanoparticles. Bulletin of the Chemical Society of Ethiopia. 35. 151-160. 10.4314/bcse.v35i1.13.

56. Dundar, Ibrahim & Mere, Arvo & Mikli, Valdek & Krunks, Malle & Oja Acik, Ilona. (2020). Thickness Effect on Photocatalytic Activity of TiO2 Thin Films Fabricated by Ultrasonic Spray Pyrolysis. Catalysts. 10. 1058. 10.3390/catal10091058.

57. Céline Dupont, Jacques Jupille, Sylvie Bourgeois, Patrick Le Fèvre, Alberto Verdini, Luca Floreano, and Bruno Domenichini Substitution of Titanium for Magnesium Ions at the Surface of Mg-Doped Rutile The Journal of Physical Chemistry C 2020 124 (21), 11490-11498 DOI: 10.1021/acs.jpcc.0c02321

58. Darmadi, I & Taufik, Ardiansyah & Saleh, Rosari. (2020). Analysis of optical and structural properties of Ti-doped ZnO nanoparticles synthesized by co-precipitation method. Journal of Physics: Conference Series. 1442. 012021. 10.1088/1742-6596/1442/1/012021.

59. Mishra, Gourav & Mukhopadhyay, Mausumi. (2019). TiO2 decorated functionalized halloysite nanotubes (TiO2@HNTs) and photocatalytic PVC membranes synthesis, characterization and its application in water treatment. Scientific Reports. 9. 1-17. 10.1038/s41598-019-40775-4.

60. Jeon, Jae Bum; Kim, Byeong Jo; Bang, Gi Joo; Kim, Min-cheol; Lee, Dong Geon; Lee, Jae Myeong; Lee, Minho; Han, Hyun Soo; Boschloo, Gerrit; Lee, Sangwook; Jung, Hyun Suk

(2019). Photo-annealed Amorphous Titanium Oxide for Perovskite Solar Cells. Nanoscale, (), 10.1039.C9NR05776E–. doi:10.1039/C9NR05776E

61. Rehab Ramadan, David Romera, Rosalía Delgado Carrascón, Miguel Cantero, John-Jairo Aguilera-Correa, Josefa P. García Ruiz, Jaime Esteban, and Miguel Manso Silván Sol–Gel-Deposited Ti-Doped ZnO: Toward Cell Fouling Transparent Conductive Oxides ACS Omega 2019 4 (7), 11354-11363DOI: 10.1021/acsomega.9b00646

62. Khan, M.I.; Farooq, W.A.; Saleem, Muhammad; Bhatti, K.A.; Atif, M.; Hanif, Atif (2019). Phase change, band gap energy and electrical resistivity of Mg doped TiO2 multilayer thin films for dye sensitized solar cells applications. Ceramics International, (), S0272884219319534–. doi:10.1016/j.ceramint.2019.07.133.

63. Lee, Dong Geon; Kim, Min-cheol; Kim, Byeong Jo; Kim, Dong Hoe; Lee, Sang Myeong; Choi, Mansoo; Lee, Sangwook; Jung, Hyun Suk (2017). Effect of TiO 2 particle size and layer thickness on mesoscopic perovskite solar cells. Applied Surface Science, (), S0169433217334050–. doi:10.1016/j.apsusc.2017.11.124

64. Wojcieszak, Damian; Mazur, Michal; Kaczmarek, Danuta; Domaradzki, Jaroslaw (). Influence of doping with Co, Cu, Ce and Fe on structure and photocatalytic activity of TiO2 nanoparticles. Materials Science-Poland, 35(4), 725–732. doi:10.1515/msp-2017-0117 .

65. Saito, Jo; Suzuki, Atsushi; Akiyama, Tsuyoshi; Oku, Takeo (2017). AIP Conference Proceedings [Author(s) THE IRAGO CONFERENCE 2016: 360 Degree Outlook on Critical Scientific and Technological Challenges for a Sustainable Society - Tokyo, Japan (1–2 November 2016)] - Doping effects of transition metal elements to titanium dioxide for perovskite solar cells. , 1807(), 020010–. doi:10.1063/1.4974792.

66. Asemi, M.; Ghanaatshoar, M. (2016). *The influence of magnesium oxide interfacial layer on photovoltaic properties of dye-sensitized solar cells. Applied Physics A, 122(9), 842–* . doi:10.1007/s00339-016-0369-0

67. Baktash, Ardeshir; Amiri, Omid; Sasani, Alireza (2016). Improve efficiency of Perovskite Solar Cells by using Magnesium Doped ZnO and TiO2 Compact Layers. Superlattices and Microstructures, (), S0749603616300271–. doi:10.1016/j.spmi.2016.01.026.

68. Zhang, Chenxi; Luo, Yudan; Chen, Xiaohong; Ou-Yang, Wei; Chen, Yiwei; Sun, Zhuo; Huang, Sumei (2016). Influence of different TiO2 blocking films on the photovoltaic performance of perovskite solar cells. Applied Surface Science, (), S0169433216305499–. doi:10.1016/j.apsusc.2016.03.093

69. N. Zhao et al., "Titanium doped Zinc-oxide based Thin Film Transistors: Optimization of the source/drain materials," 2014 12th IEEE International Conference on Solid-State and Integrated Circuit Technology (ICSICT), 2014, pp. 1-3, doi: 10.1109/ICSICT.2014.7021274.

70. Liu, QiuPing (2014). Photovoltaic Performance Improvement of Dye-Sensitized Solar Cells Based on Mg-Doped TiO2 Thin Films. Electrochimica Acta, 129(), 459–462. doi:10.1016/j.electacta.2014.02.129

71. Mohammad A. Behnajady; Bahare Alizade; Nasser Modirshahla (2011). Synthesis of Mg-Doped TiO2 Nanoparticles under Different Conditions and its Photocatalytic Activity. , 87(6), 1308–1314. doi:10.1111/j.1751-1097.2011.01002.x.

72. Olea, Javier & Toledano-Luque, M. & Pastor, D. & González-Díaz, G. & Mártil, Ignacio. (2008). Titanium doped silicon layers with very high concentration. Journal of Applied Physics. 104. 016105 - 016105. 10.1063/1.2949258.

73. Devi, Maya & Panigrahi, Manas. (2015). SYNTHESIS AND CHARACTERIZATION OF Mg DOPED TiO2 THIN FILM FOR SOLAR CELL APPLICATION. International Journal Of Engineering & Applied Sciences. 7. 1-1. 10.24107/ijeas.251250.

74. https://www.differencebetween.com/difference-between-rutile-and-anatase-titanium-dioxide/